MEMS and biological cells – advances in designing sensors, actuators and biocompatible surfaces for medical use

Richard Funk, TU-Dresden

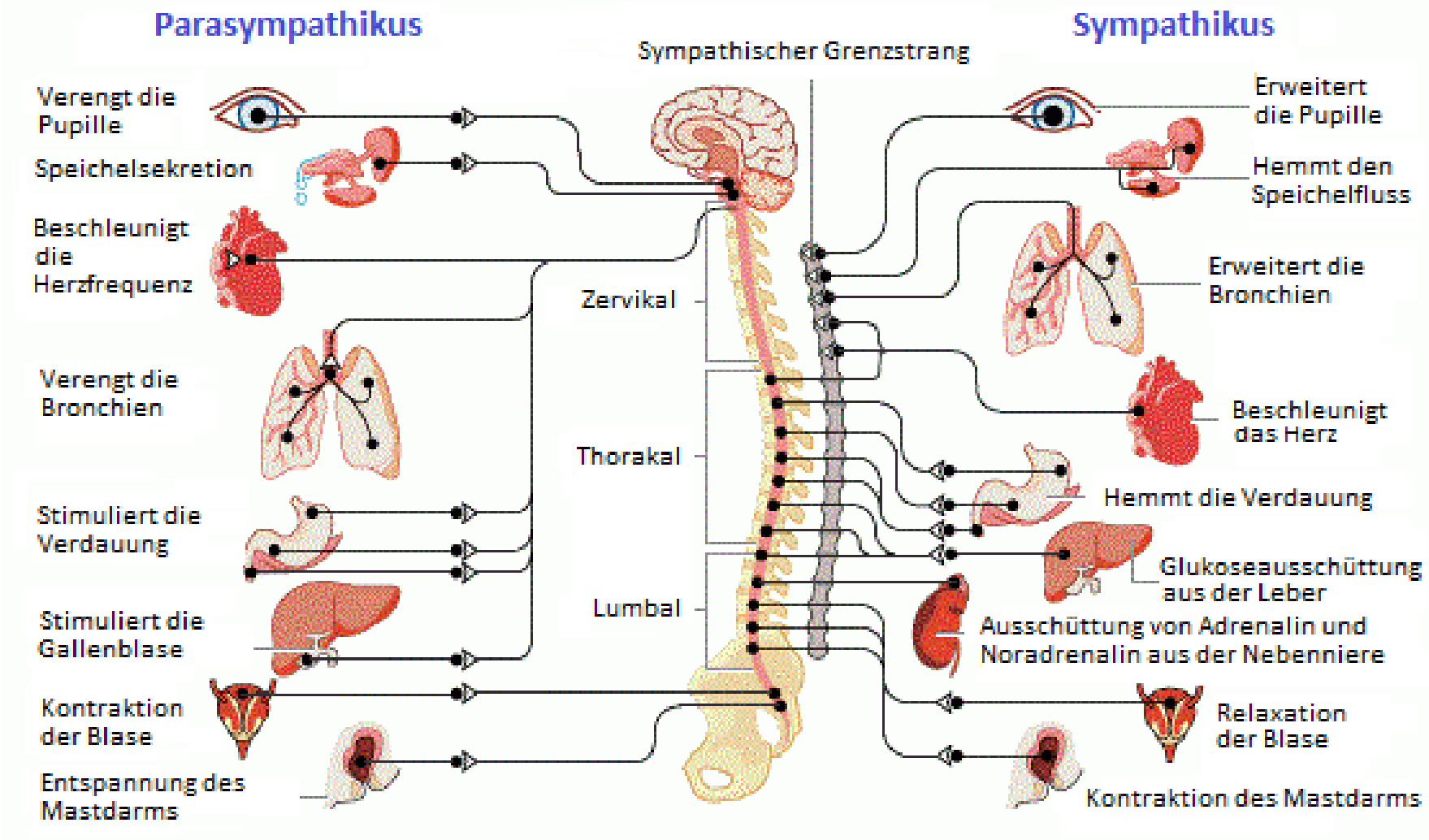
Parasympathikus
Sympathikus
Sympathischer Grenzstrang
Verengt die Pupille
Speichelsekretion
Beschleunigt die Herzfrequenz
Verengt die Bronchien
Stimuliert die Verdauung
Stimuliert die Gallenblase
Kontraktion der Blase
Entspannung des Mastdarms
Zervikal
Thorakal
Lumbal
Erweitert die Pupille
Hemmt den Speichelfluss
Erweitert die Bronchien
Beschleunigt das Herz
Hemmt die Verdauung
Glukoseausschüttung aus der Leber
Ausschüttung von Adrenalin und Noradrenalin aus der Nebenniere
Relaxation der Blase
Kontraktion des Mastdarms

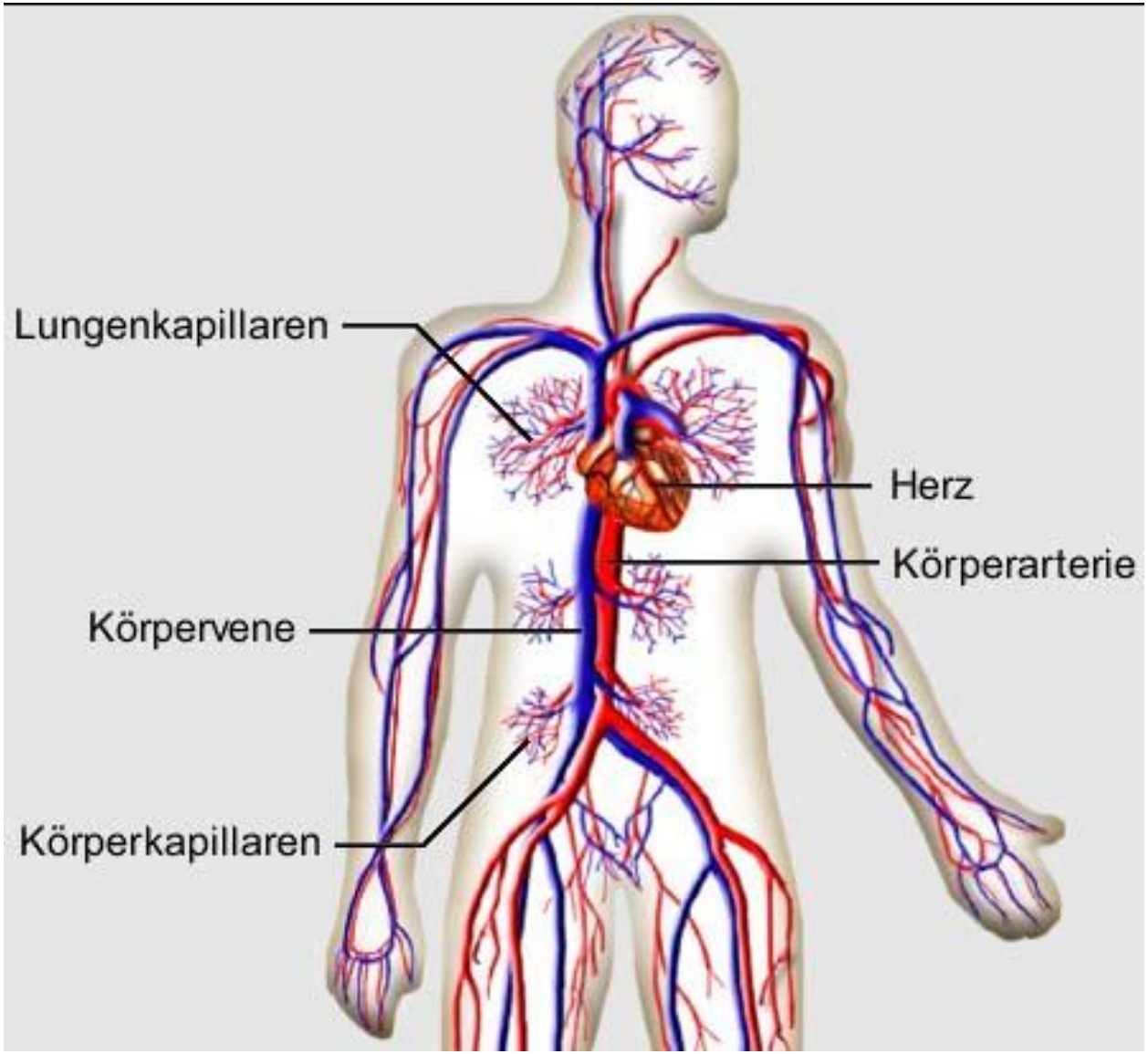

Blutfluss,
Druckverlauf,
Puls,
O2, CO2, alle
Blutparameter,
Hormone etc.

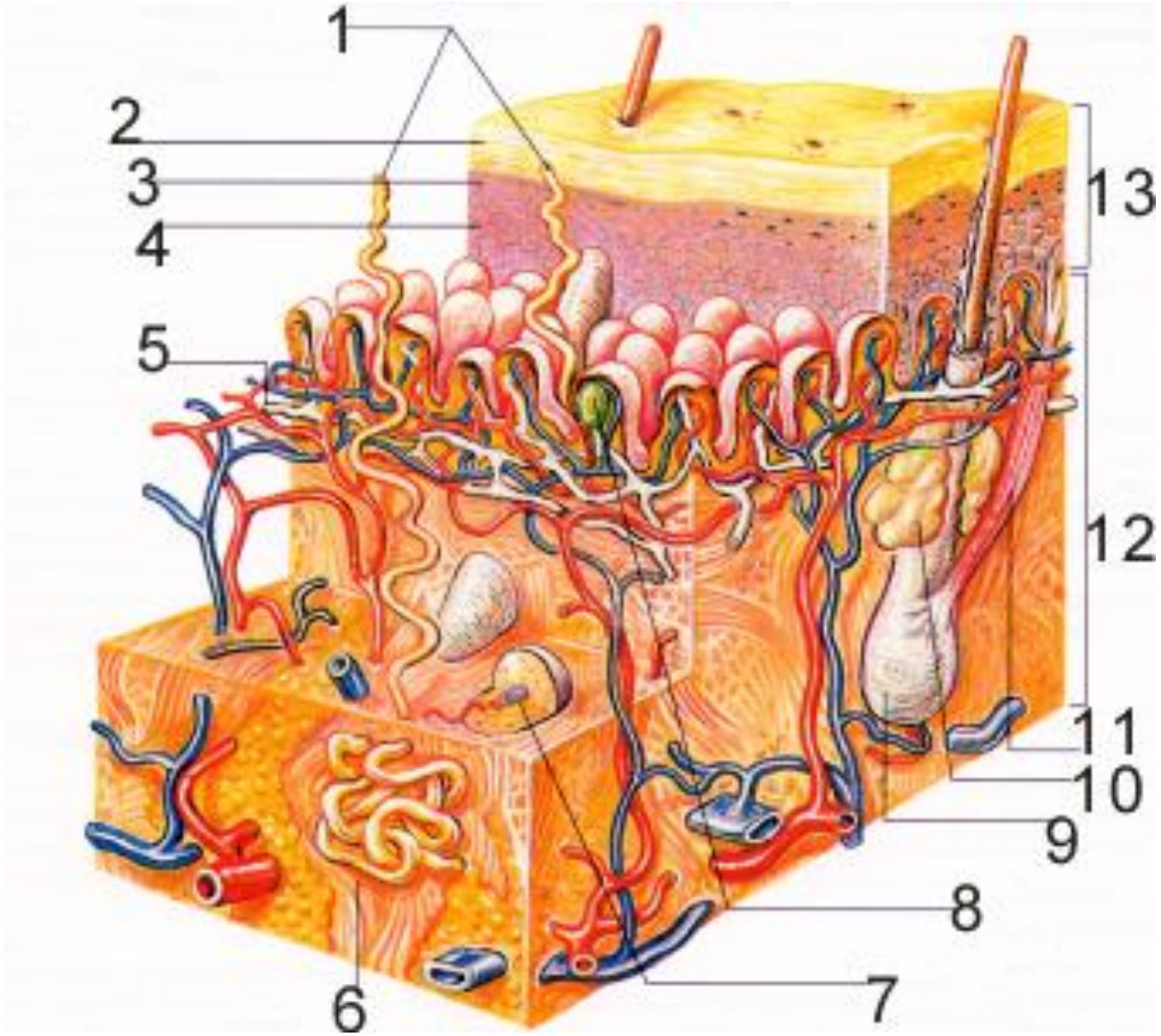
1
2
3
4
5
6
7
8
9
10
11
12
13


How to analyze this complex array of different components found in tissues?
© Cassella-Riedel

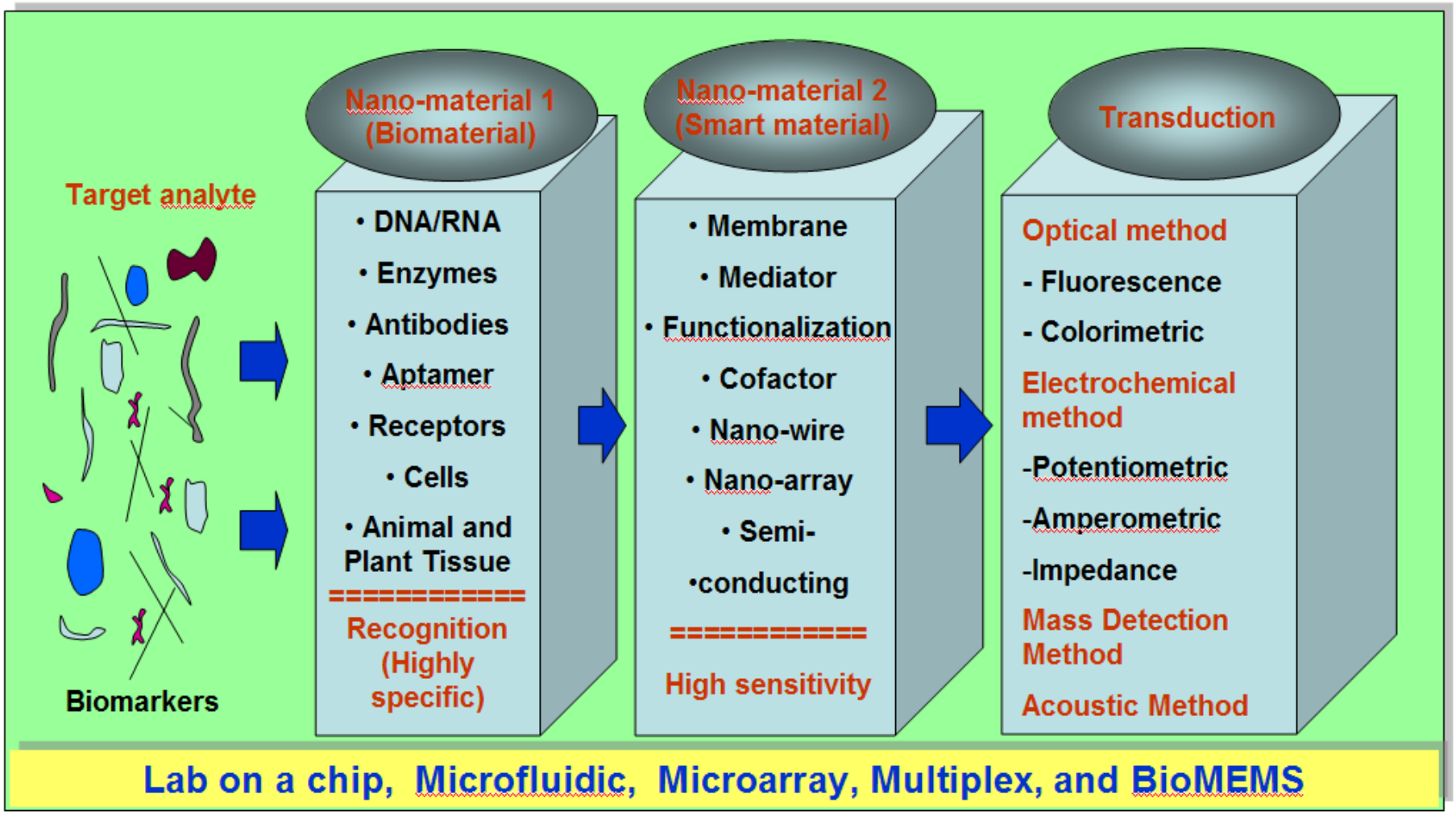

Yun YH, Eteshola E, Bhattacharya A, Dong Z, Shim JS, Conforti L, Kim D, Schulz MJ, Ahn CH, Watts N. Tiny medicine: nanomaterial-based biosensors. Sensors (Basel). 2009;9(11):9275-99

Technology News
Wireless transceiver circuit enables low-power medical body area networks, EE Times
February 12, 2014 | Jean-Pierre Joosting | 222907618

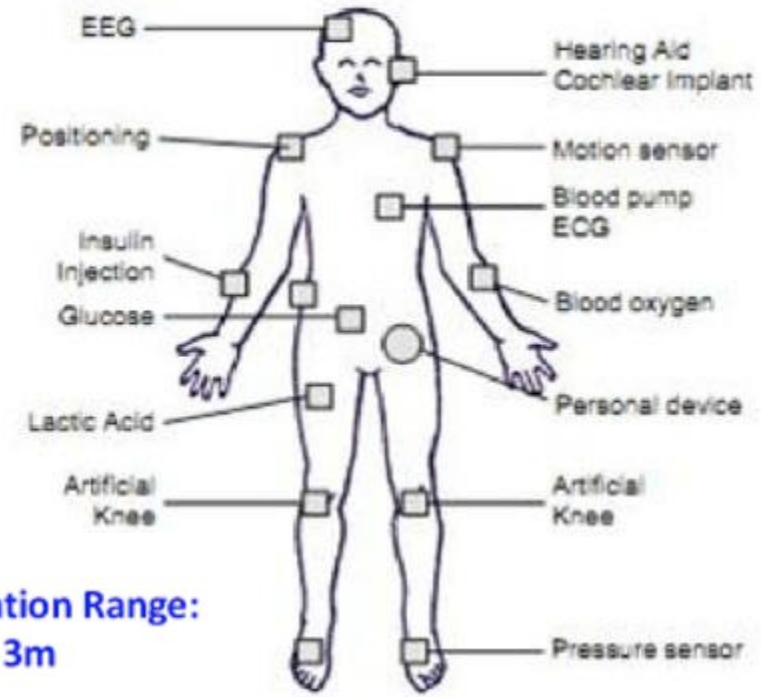

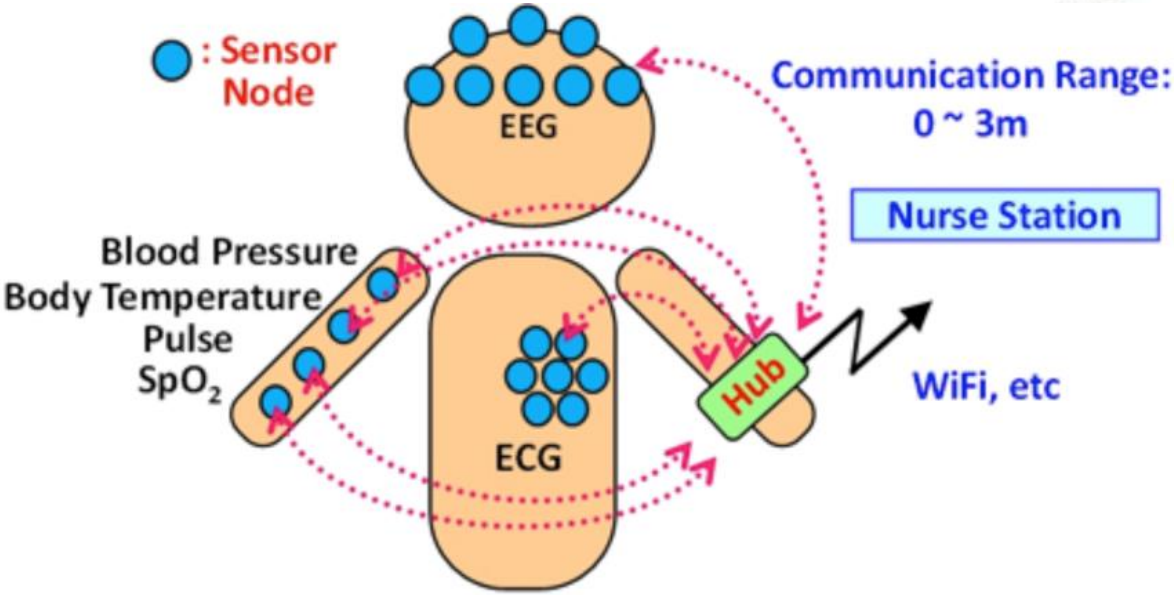

EEG: Electroencephalogram, ECG: Electrocardiogram,
SpO2: Saturation of peripheral oxygen

(a) biosensor, (b) protein absorption, (c) cell deposition, and (d) fibrosis and angiogenesis

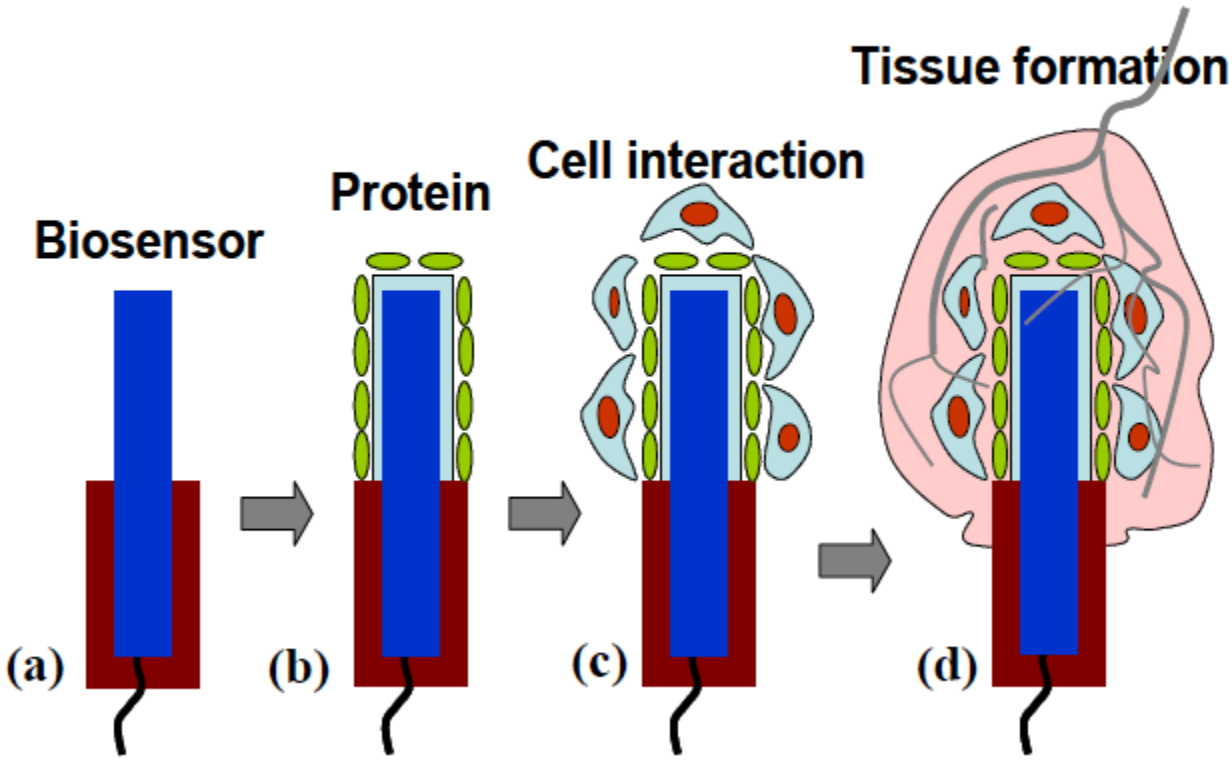

Yun YH, Eteshola E, Bhattacharya A, Dong Z, Shim JS, Conforti L, Kim D, Schulz MJ, Ahn CH, Watts N. Tiny medicine: nanomaterial-based biosensors. Sensors (Basel). 2009;9(11):9275-99

Smart lens

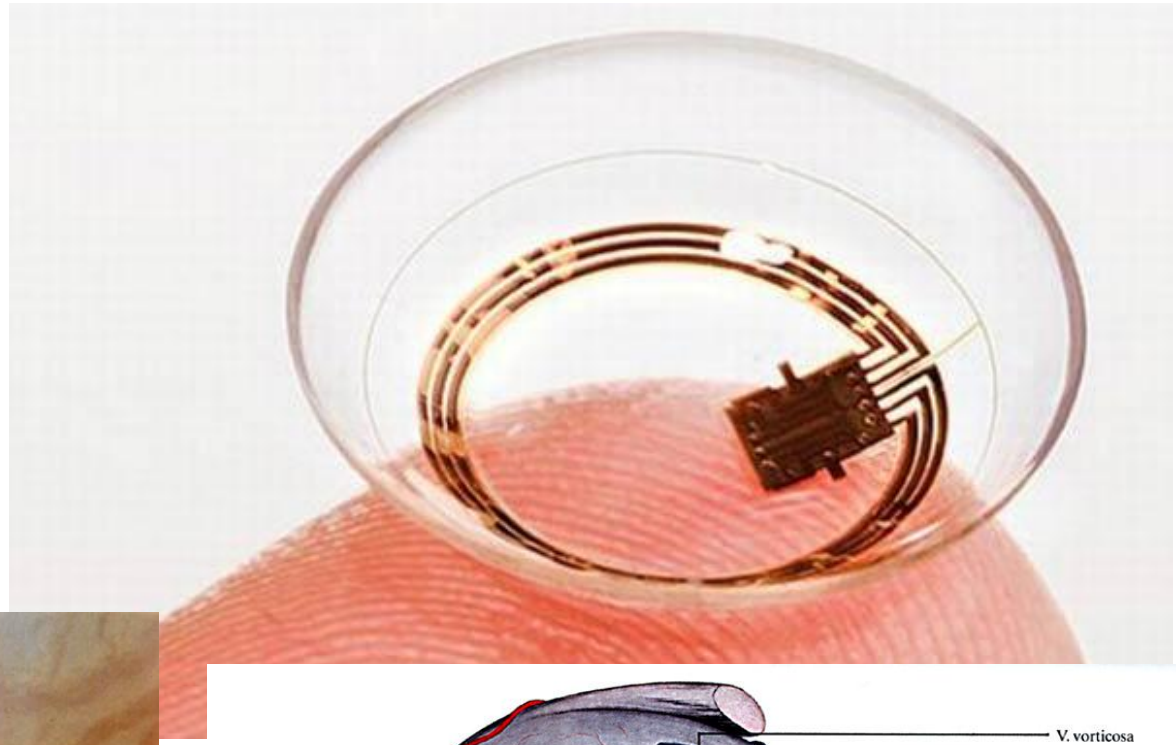

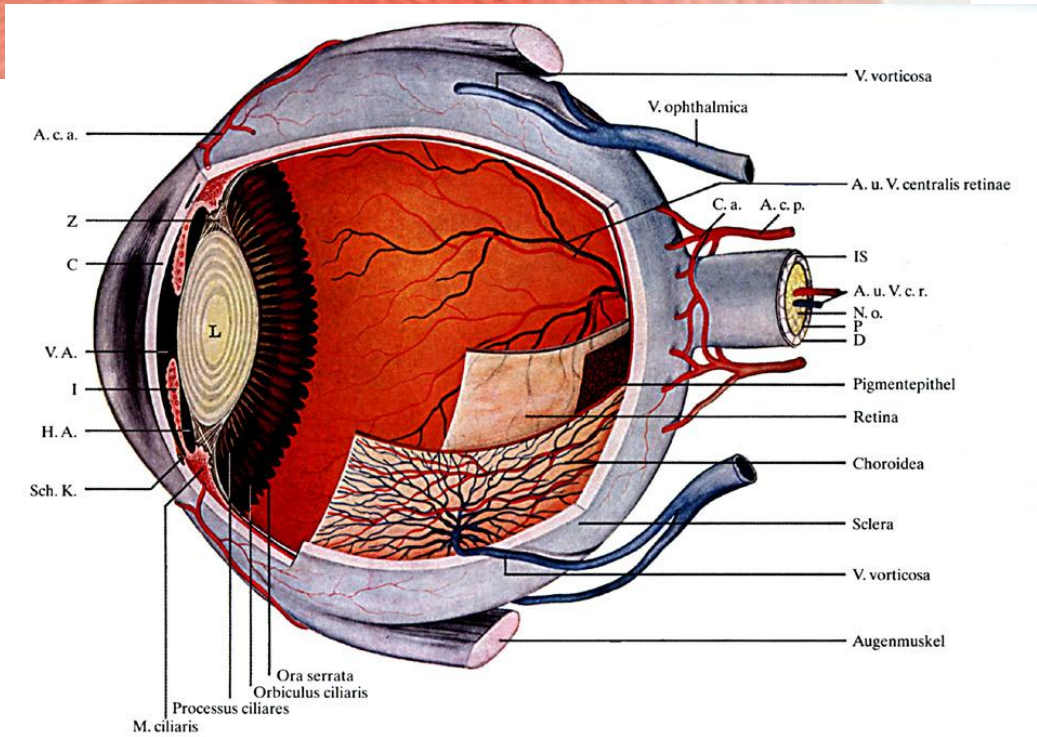
V. vorticosa
V. ophthalmica
A. c. a.
A. u. V. centralis retinae
C. a.
A. c. p.
Z
C
IS
A. u. V. c. r.
N. o.
P
D
L
V. A.
I
Pigmentepithel
H. A.
Retina
Choroidea
Sch. K.
Sclera
V. vorticosa
Augenmuskel
Ora serrata
Orbiculus ciliaris
Processus ciliares
M. ciliaris


0
1
2
3
4
5
6
7


Move and Scale
Analysis
Archive
Low Risk Lesion
Archive it and keep track of its evolution
No additional information.
Find Nearby Doctors


Patient: Unknown Operator: Unknown
Delete
Done
Adjust

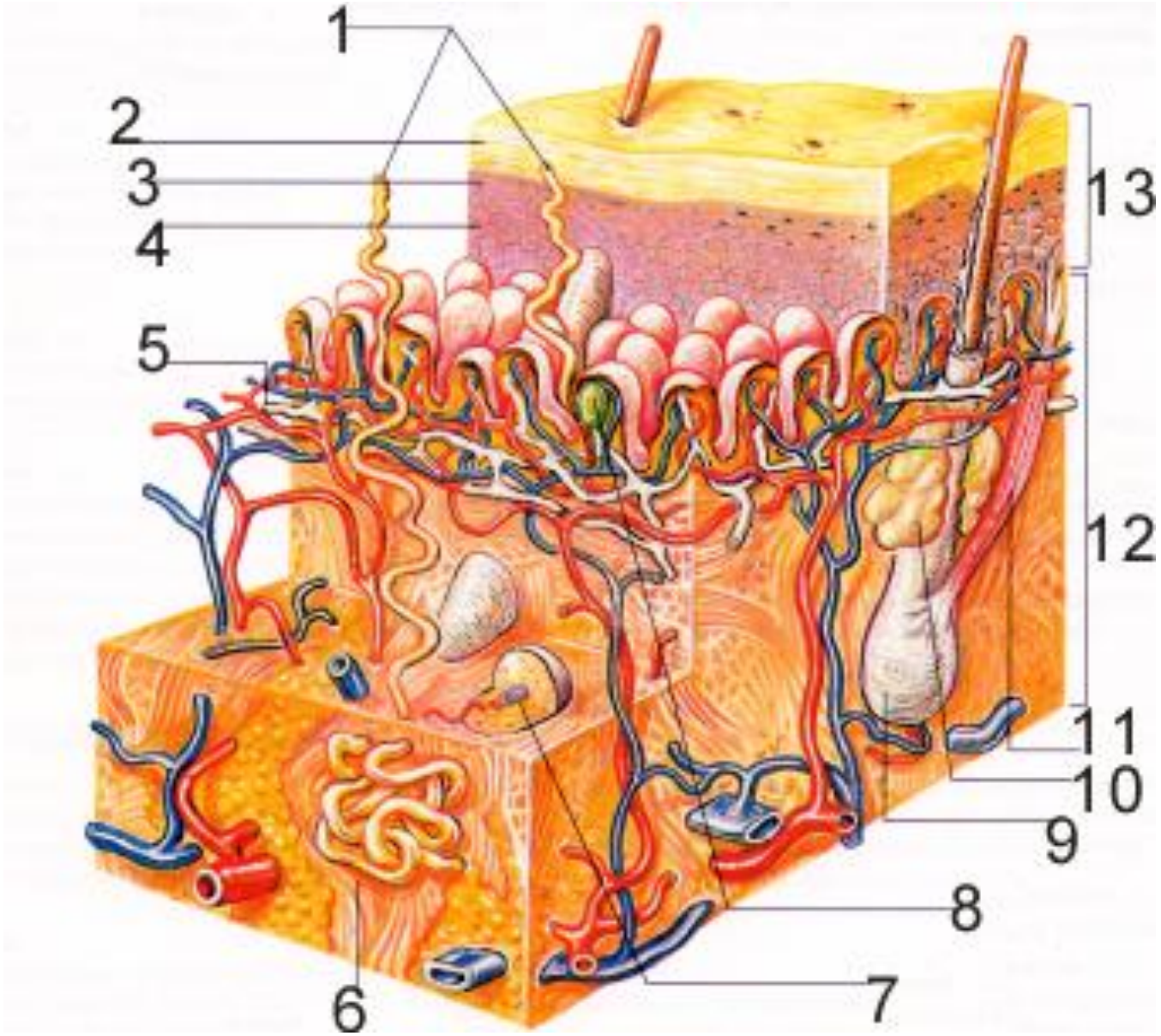
1
2
3
4
5
6
7
8
9
10
11
12
13

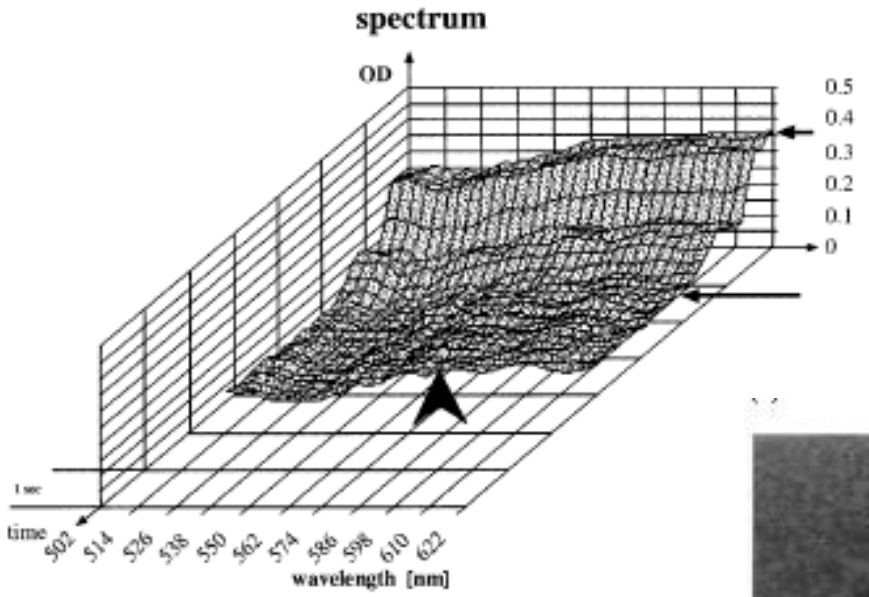

We could also measure cytochrome c spectra out of living cells

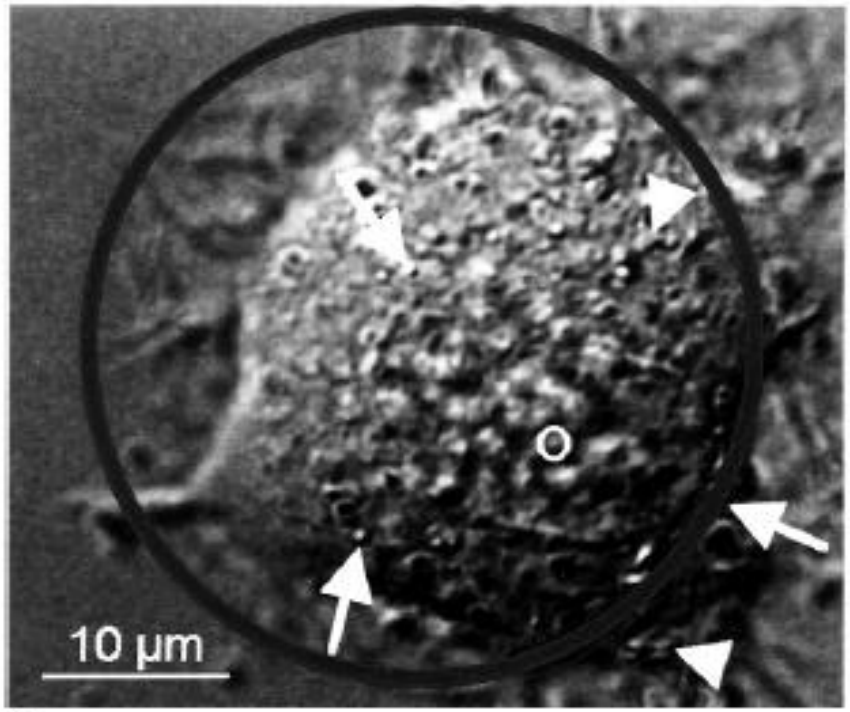

(*b*)

Figure 4. (*a*) Spectra of buffer solution alone (short arrow) and buffer solution with NG 108-15 cells (long arrow) placed in the VECM microchamber. Several peaks, also of cytochrome c at 550 nm (arrowhead) are detectable. (*b*) VECM picture of NG 108-15 cell showing mitochondria (arrowheads), vacuoles (arrows) and the nucleus (circle). The large circle indicates the area of spectrophotometric measurement.

R H W Funk , J Höper , P Dramm and A Hofer

Physiol. Meas. **19** 225-233, 1998

- oxidiertes Cytochrom C und reduziertes Cytochrom C zeigen unterschiedliche Absorptionsspektren:

  Extinktionsverhältnisse geben reduzierten Cytochrom C Gehalt wieder

  → Nutze optische Filter mit charakteristischen Wellenlängen für separate Kamerabilder

  → ortsaufgelöste Darstellung des reduzierten Cytochrom Cs

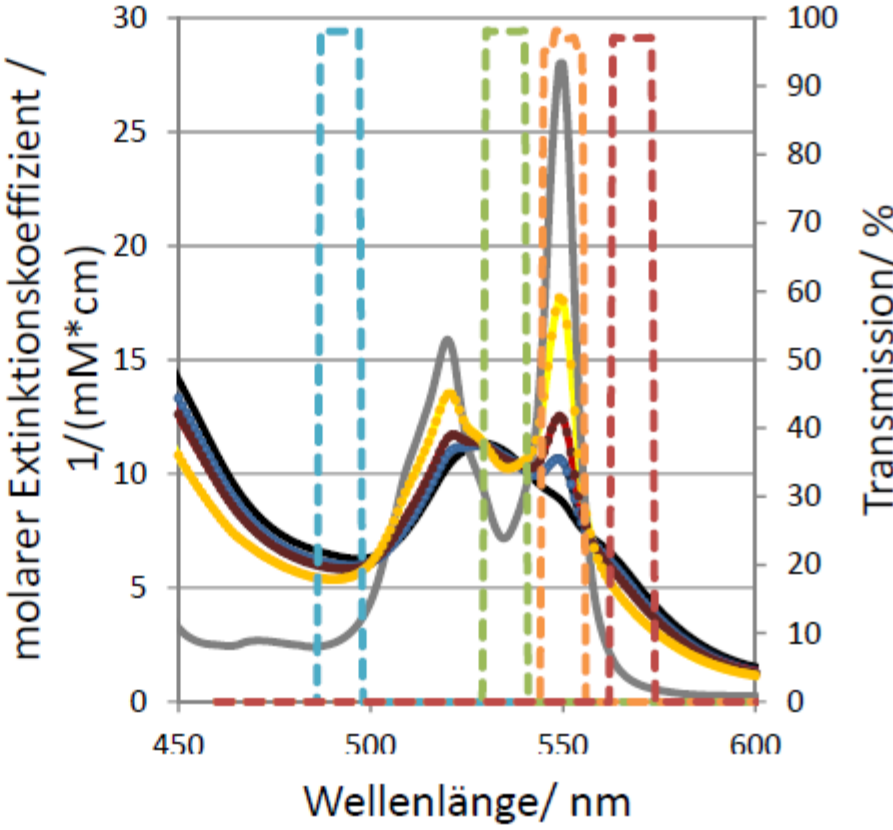

Extinktionsberechnung – qualitative Auswertung

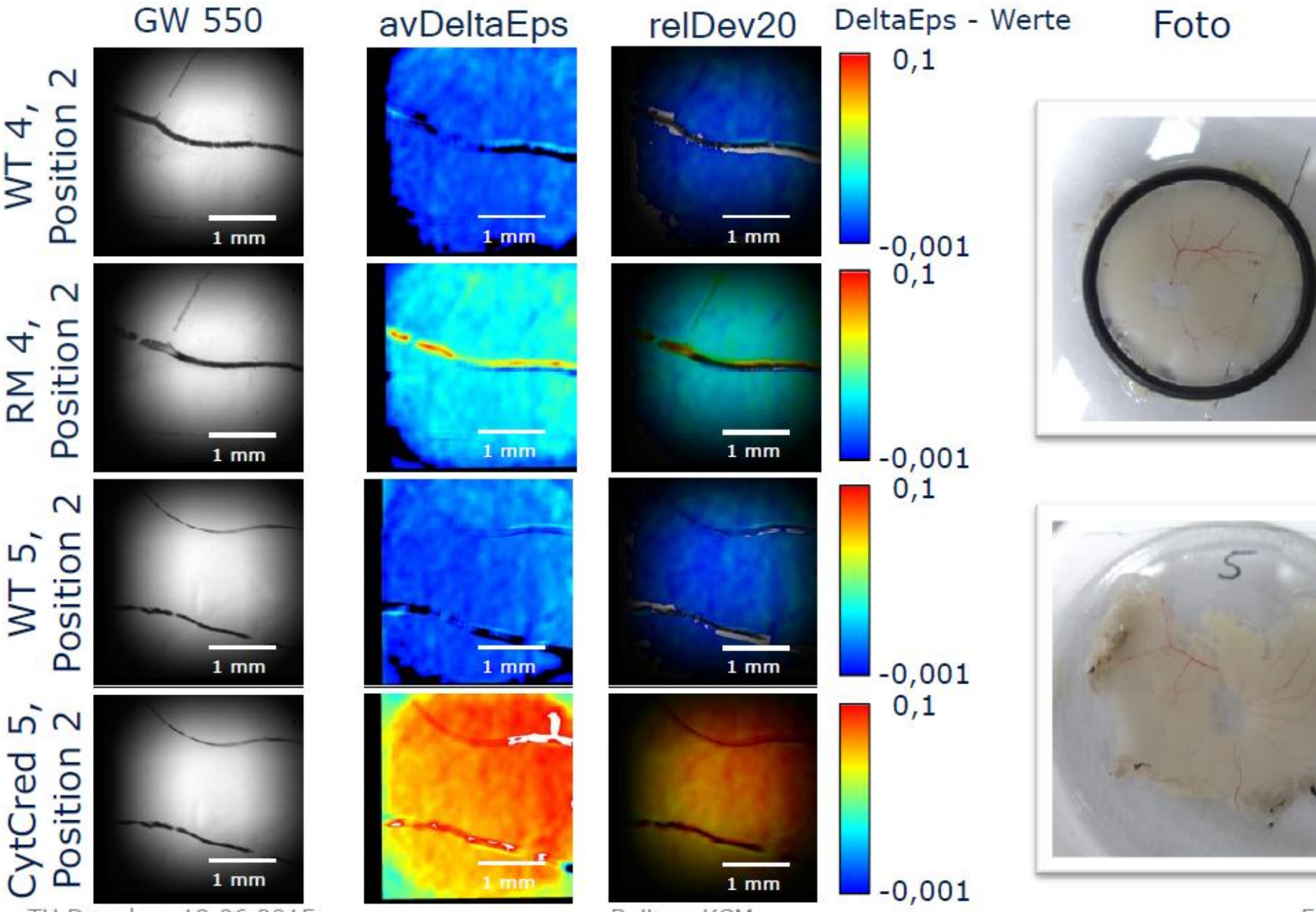

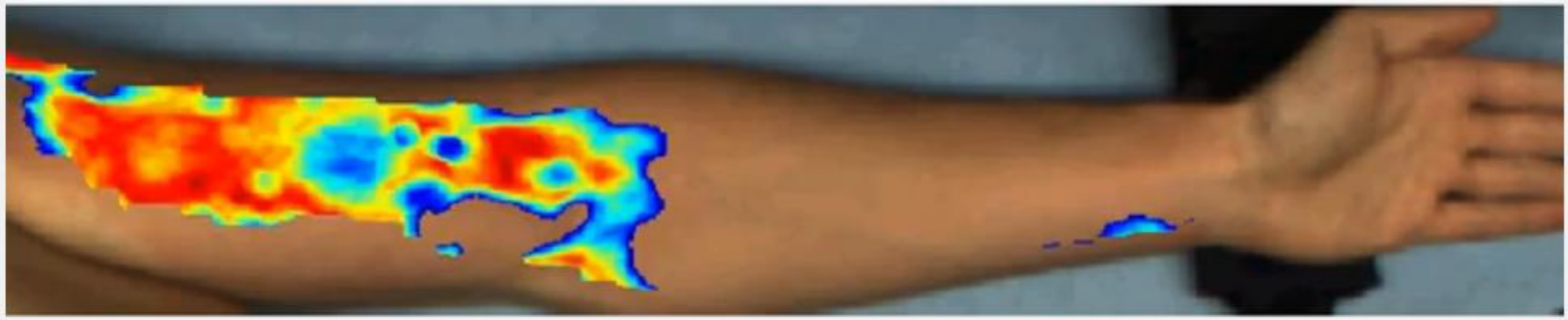

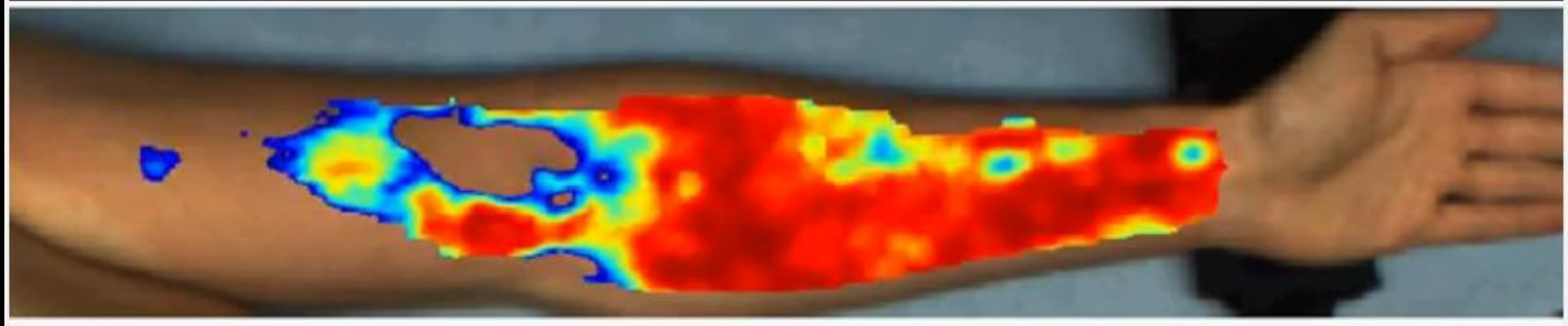

1. Untersuchungen an Probanden *in vivo*

Untersuchung der Durchblutung der Finger mittels Laser-Doppler

Kontrolle

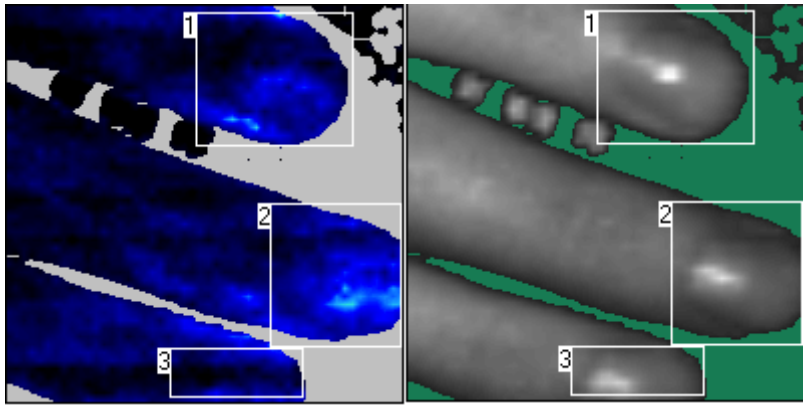

direkt nach
1x MagCell

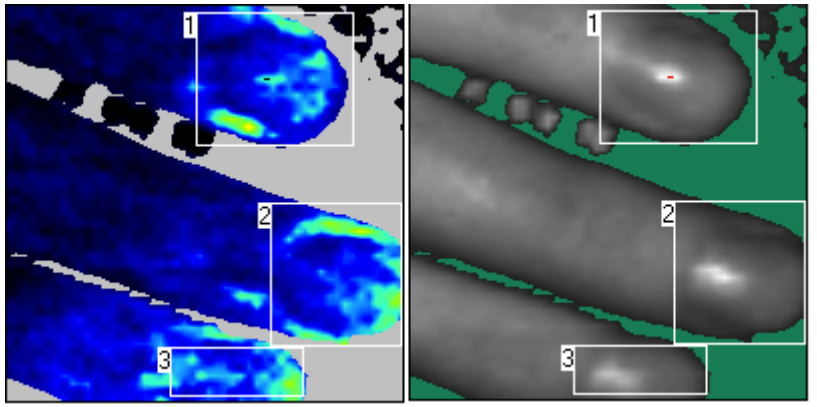

Behandlung
mit rotem Licht

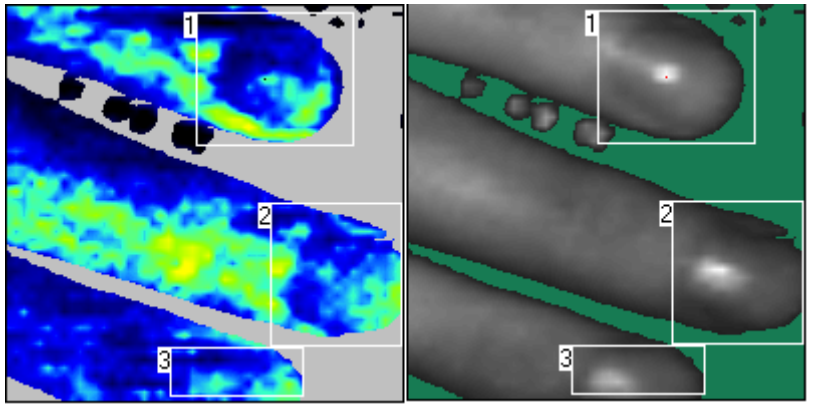

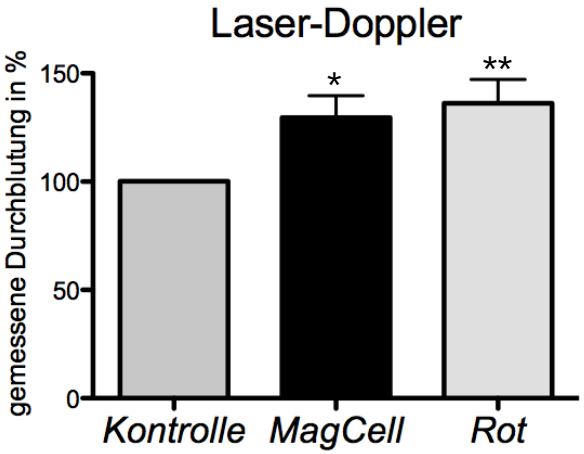

1. Untersuchungen an Probanden *in vivo*

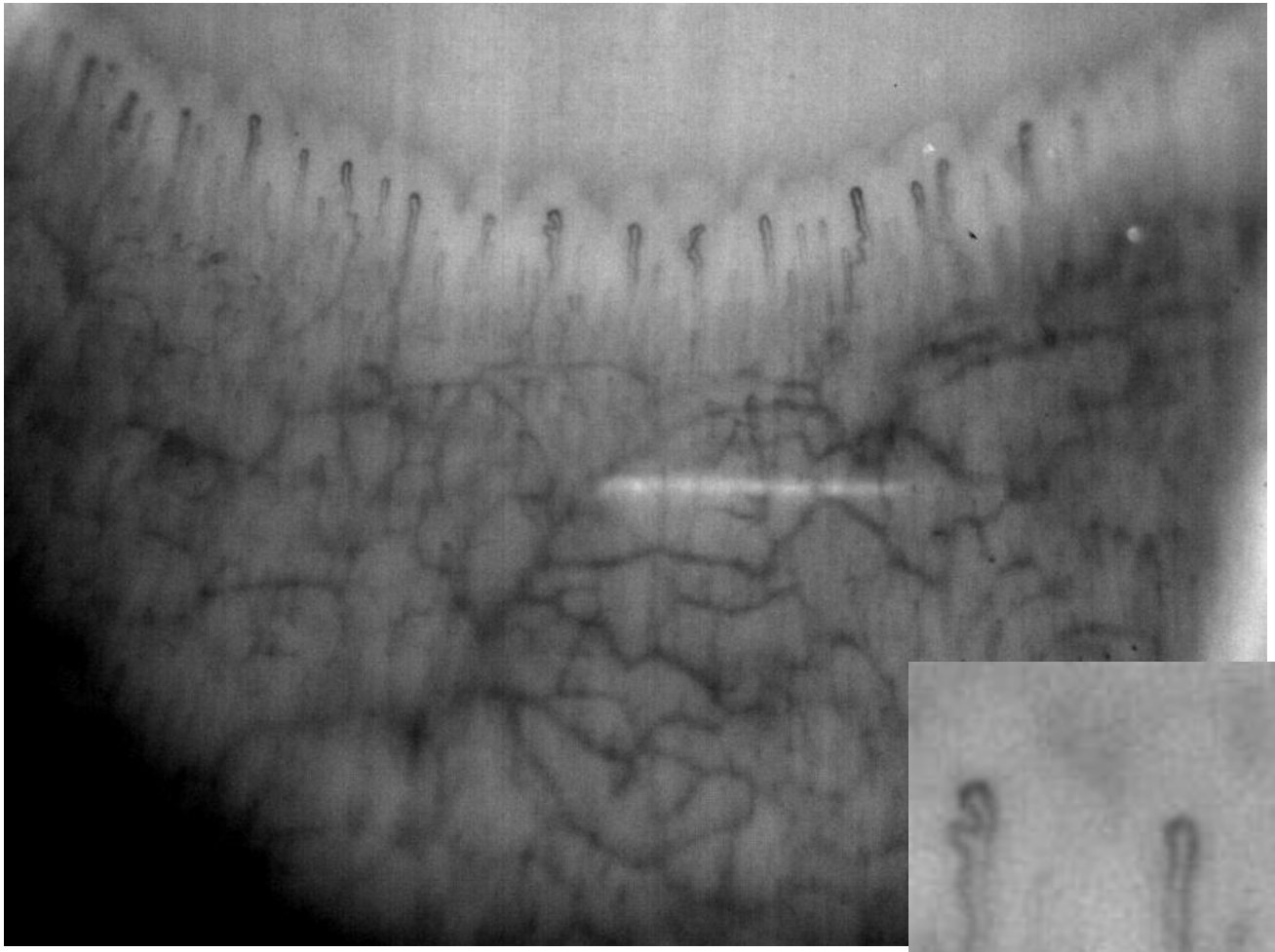

Untersuchung zur Wirkung der Magcell Behandlung auf die Durchblutung/ Mikrozirkulation der Nagelfalzkapillaren

Kapillaren der Nagelfalz

Versuchsreihe läuft noch

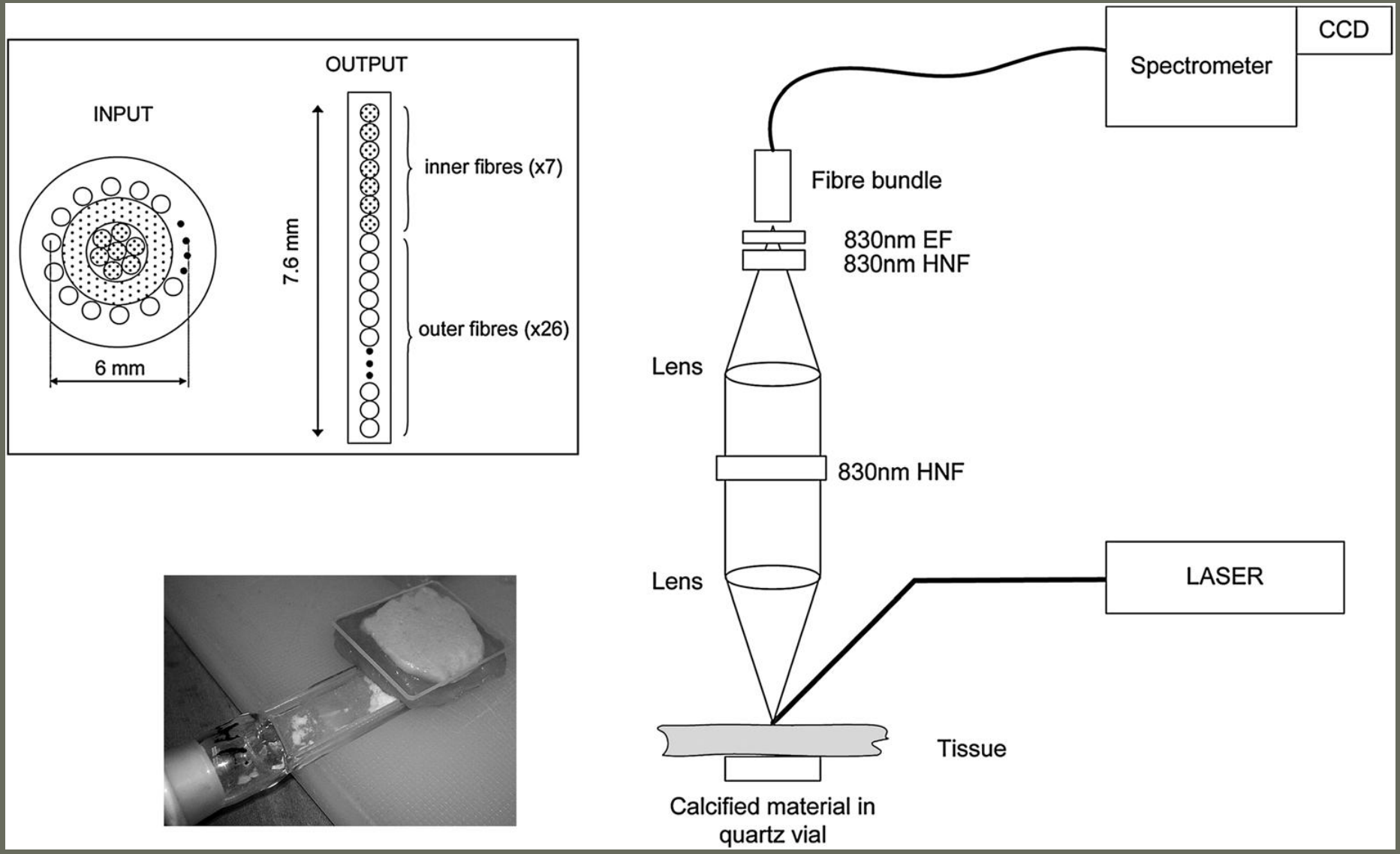

Emerging concepts in **deep Raman spectroscopy of biological tissue**
Pavel Matousek and Nicholas Stone
First published as an Advance Article on the web 17th February 2009

Journal of Biomedical Optics 19(11), 111603 (November 2014)

Raman spectroscopy: in vivo quick response code of skin physiological status

,

Raoul Vyumvuhore, Ali Tfayli, Olivier Piot, Maud Le Guillou, Nathalie Guichard, Michel Manfait, and Arlette Baillet-Guffroya

Raman-Mapping von Zellen im Medium

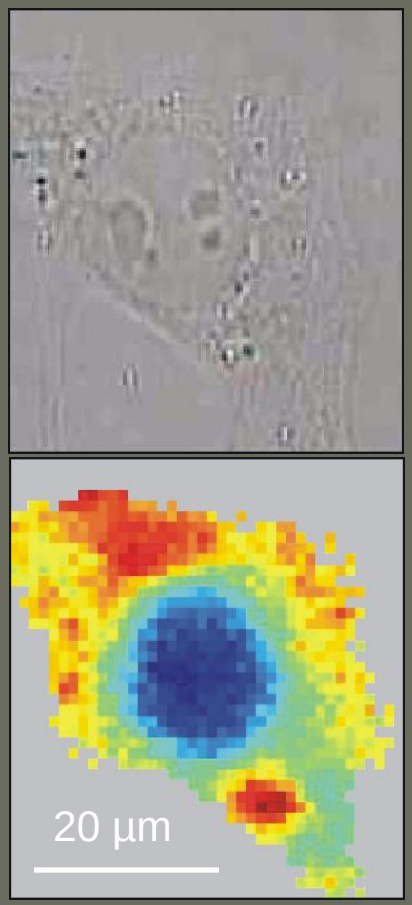

+

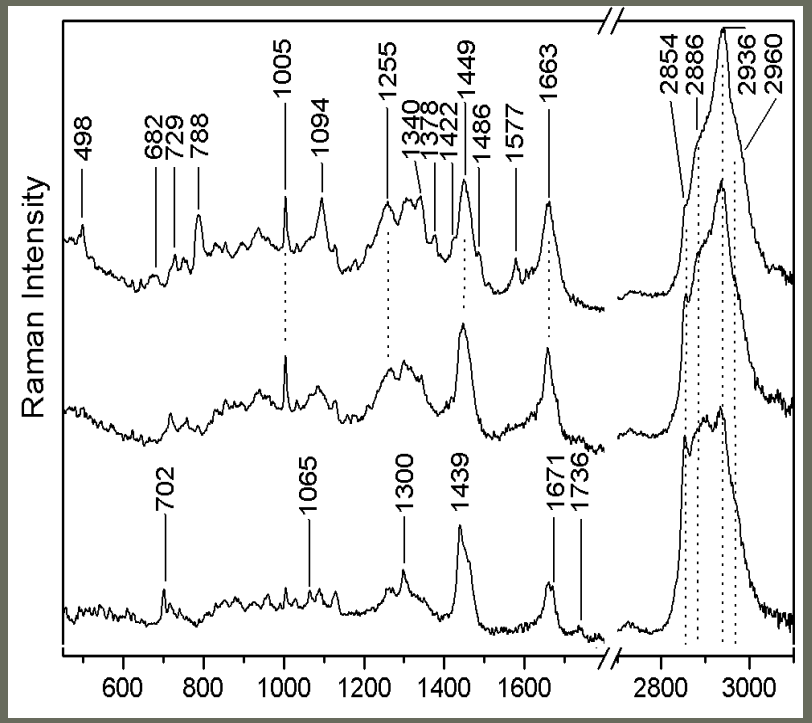

Fixierte Lungenfibroblast-Zelle in Medium.
Oben: Lichtmikroskopische Aufnahme.
Unten: Score-Plot einer PCA von Raman-Spektren.

Studies on stress-induced changes at the subcellular level by **Raman microspectroscopic mapping.**
Krafft C, Knetschke T, Funk RH, Salzer R.
Anal Chem. 2006 Jul 1;78(13):4424-9.

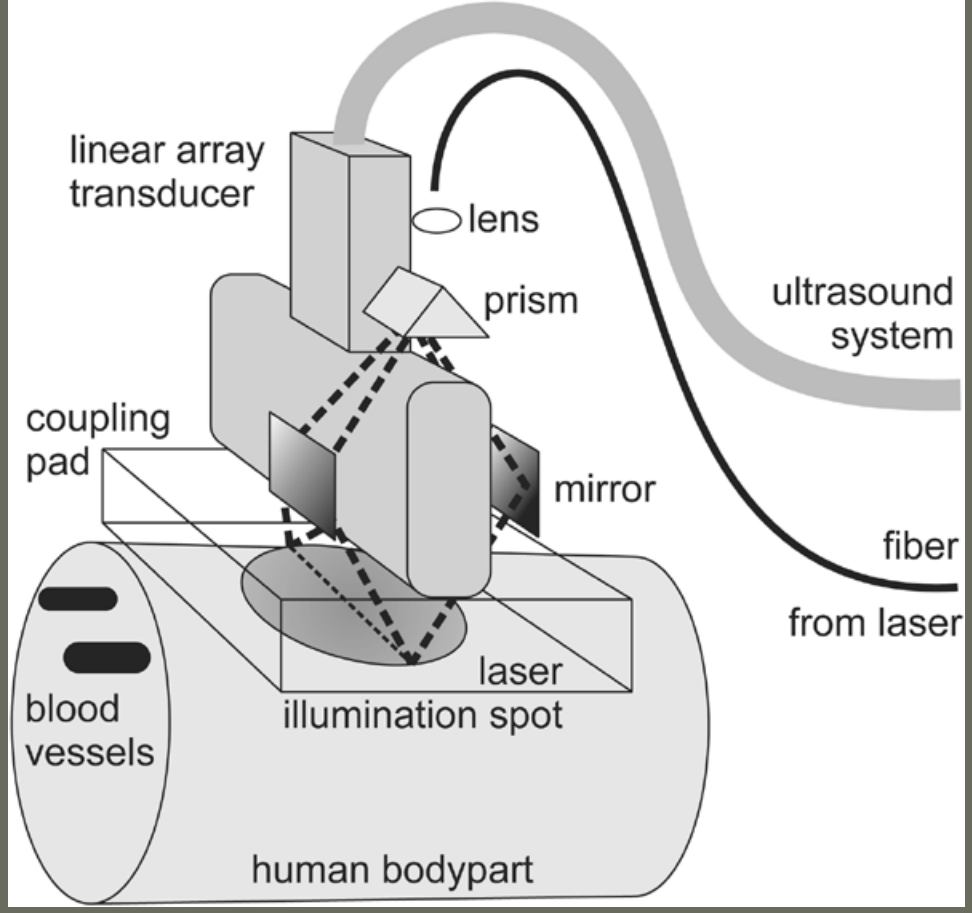

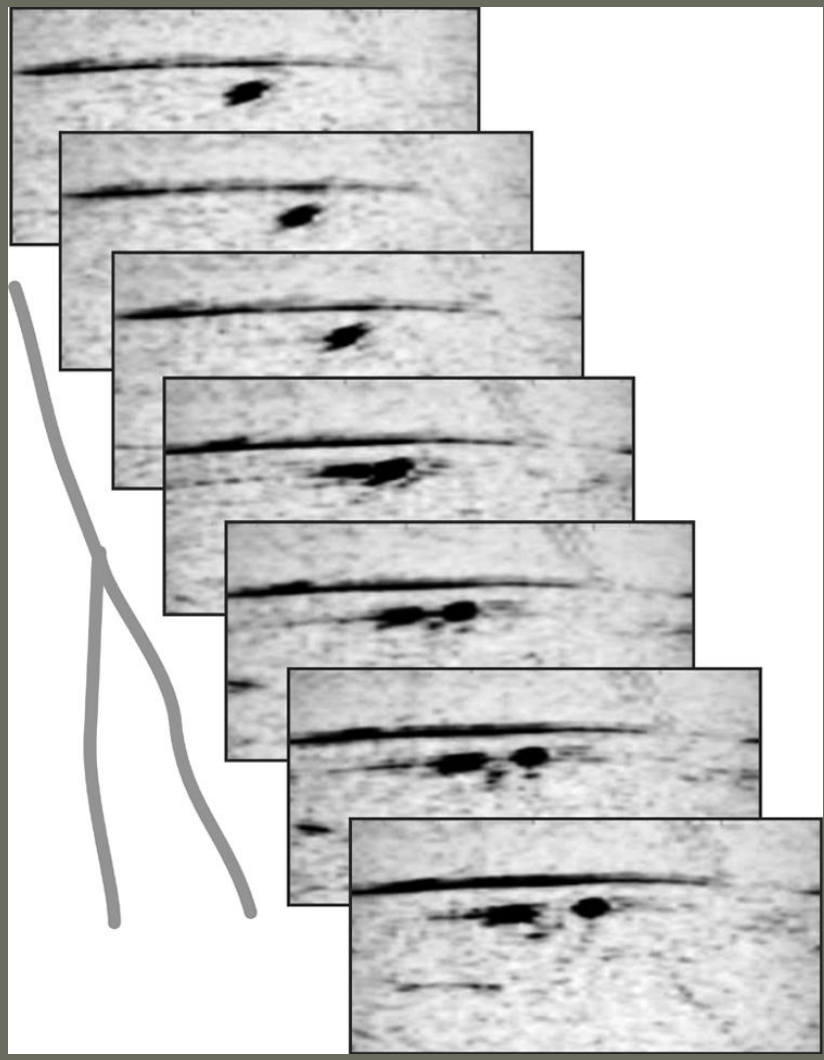

IEEE TRANSACTIONS ON MEDICAL IMAGING, VOL. 24, NO. 4, APRIL 2005
Combined **Ultrasound and Optoacoustic System** for Real-Time High-Contrast Vascular Imaging *in Vivo*
Joël J. Niederhauser, Michael Jaeger, Robert Lemor, Peter Weber, and Martin Frenz

Live cell imaging of mitochondria; JC-1

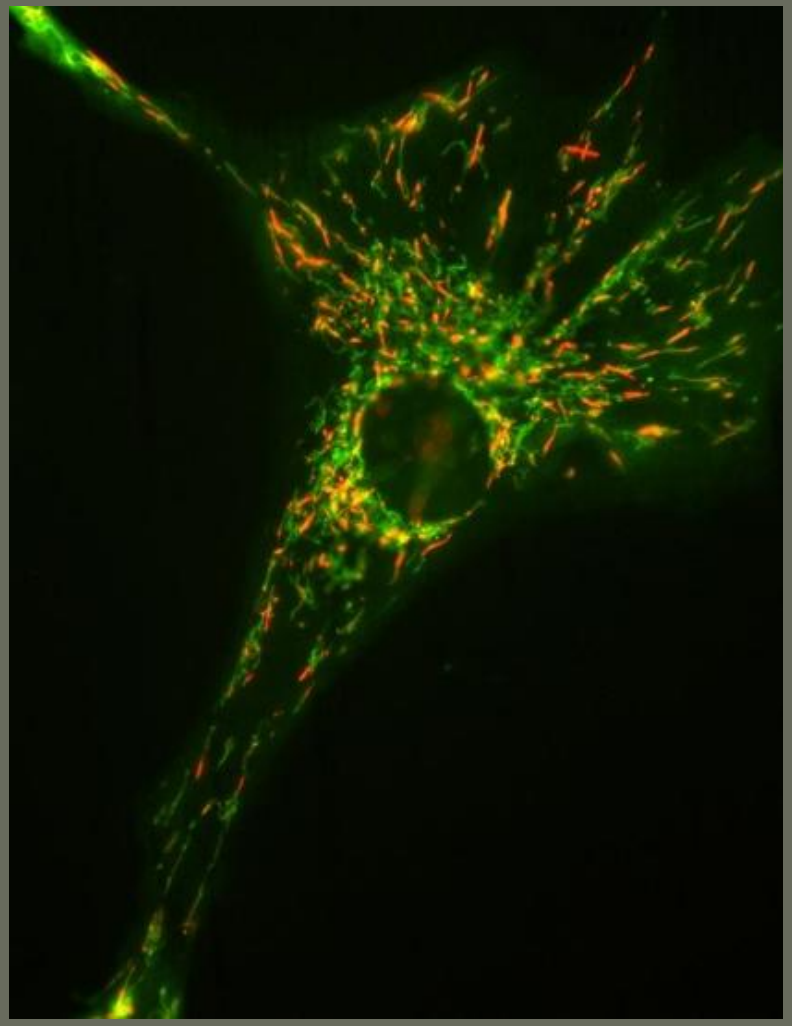

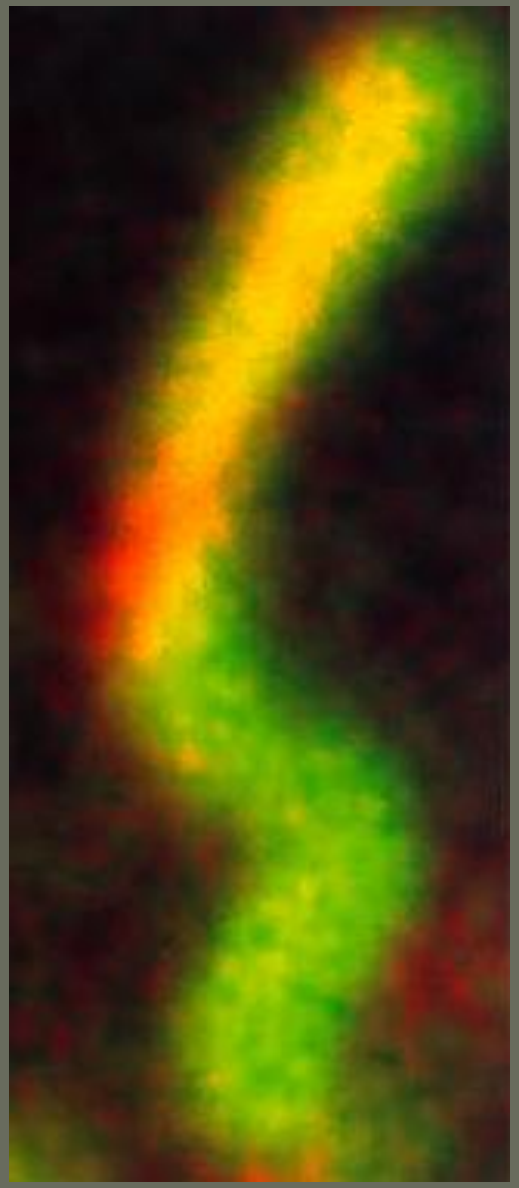

Kniep, Roehlecke, Funk et al., IOVS, **2006**

Vanishing "tattoo" multi-sensor for biomedical diagnostics

E. Moczko, I. Meglinski, S. Piletsky
Cranfield Health, Cranfield University, Silsoe, UK; 2014

ABSTRACT

Currently, precise non-invasive diagnostics systems for the real-time multi detection and monitoring of physiological parameters and chemical analytes in the human body are urgently required by clinicians, physiologists and bio-medical researchers. We have developed a novel cost effective smart ‘vanishing tattoo’ (similar to temporary child’s tattoos) consisting of environmental-sensitive dyes. Painlessly impregnated into the skin the smart tattoo is capable of generating optical/fluorescence changes (absorbance, transmission, reflectance, emission and/or luminescence within UV, VIS or NIR regions) in response to physical or chemical changes. These changes allow the identification of colour pattern changes similar to *bar-code* scanning. Such a system allows an easy, cheap and robust comprehensive detection of various parameters and analytes in a small volume of sample (e.g. variations in pH, temperature, ionic strength, solvent polarity, presence of redox species, surfactants, oxygen).

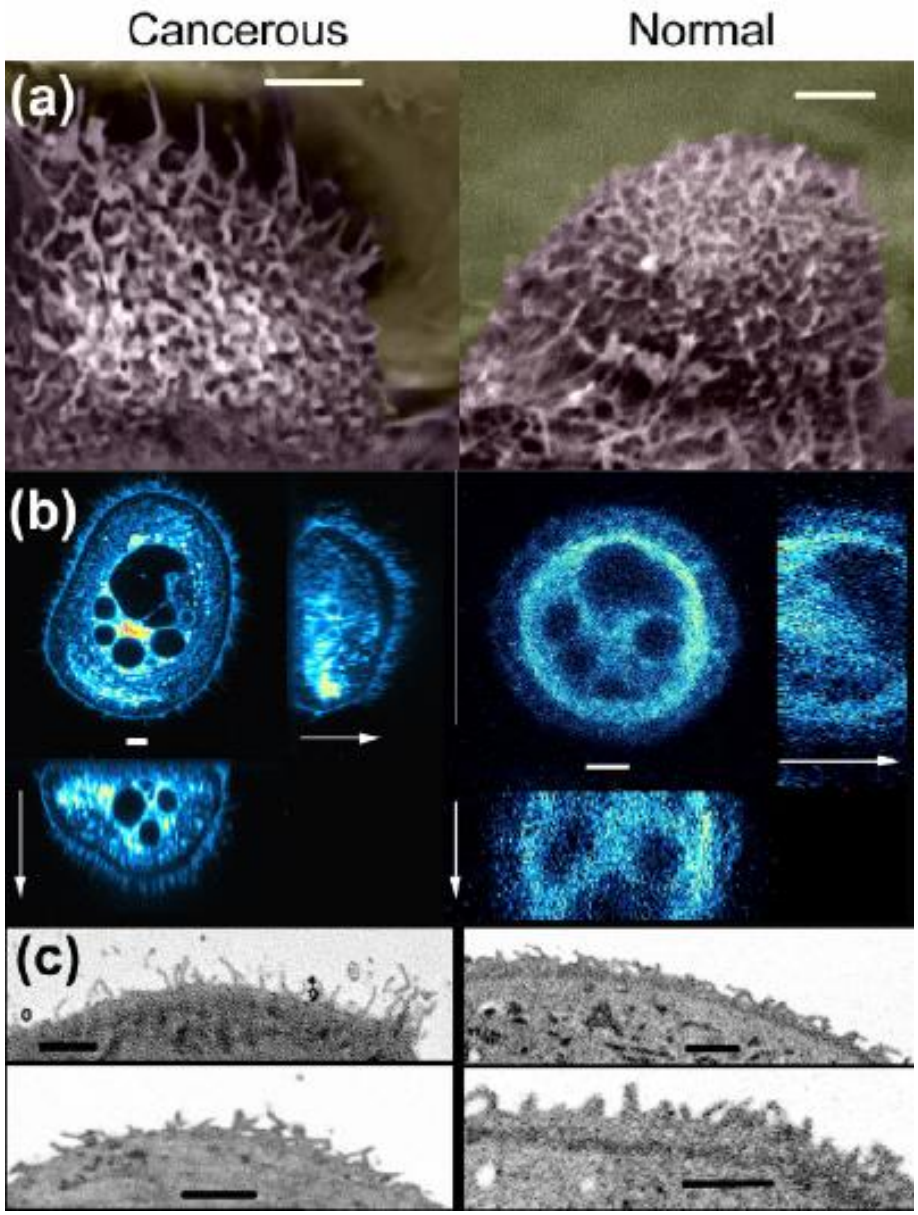

Apr 23, 2009

AFM reveals "hidden" differences between normal and cancerous cells

Using an atomic force microscope, researchers at Clarkson University in New York have identified an important difference in the surface properties of normal and cancer cells. Igor Sokolov and colleagues have found that normal cells have "brushes" of one length on their surface while cancerous cells have two brush lengths that have very different densities to the brushes on normal cells. This important variation **means that cancer and normal cells may interact very differently with nanoparticles**, something that could be exploited for cancer detection and treatment via drug delivery.

But let us go to the cell – how is the picture today and what will be new and relevant for biomedical diagnosis and therapy?

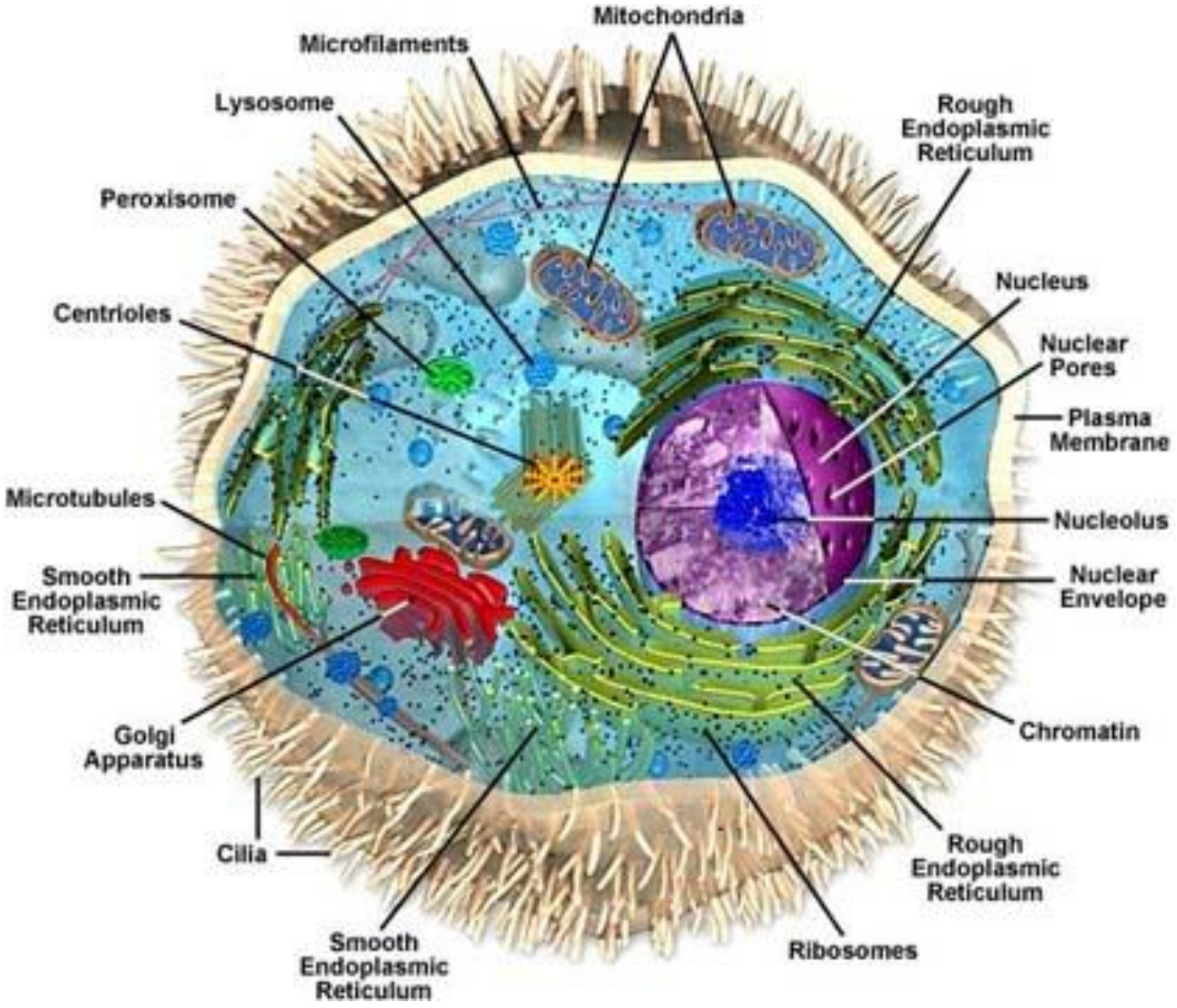

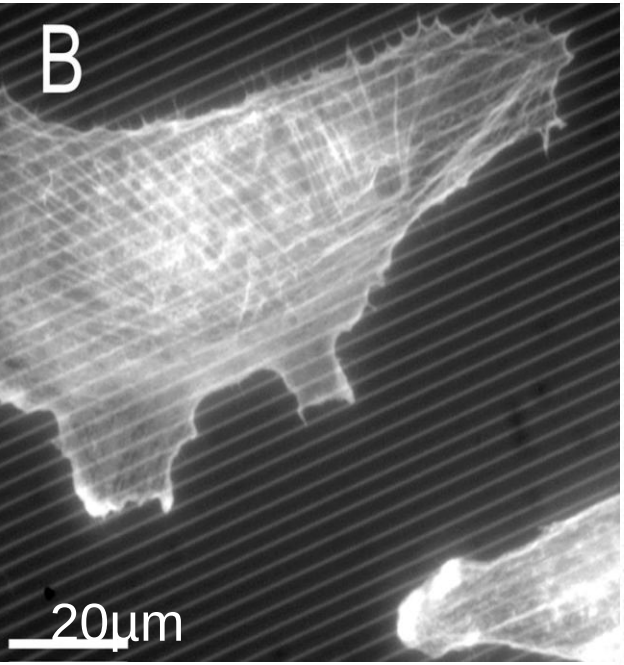

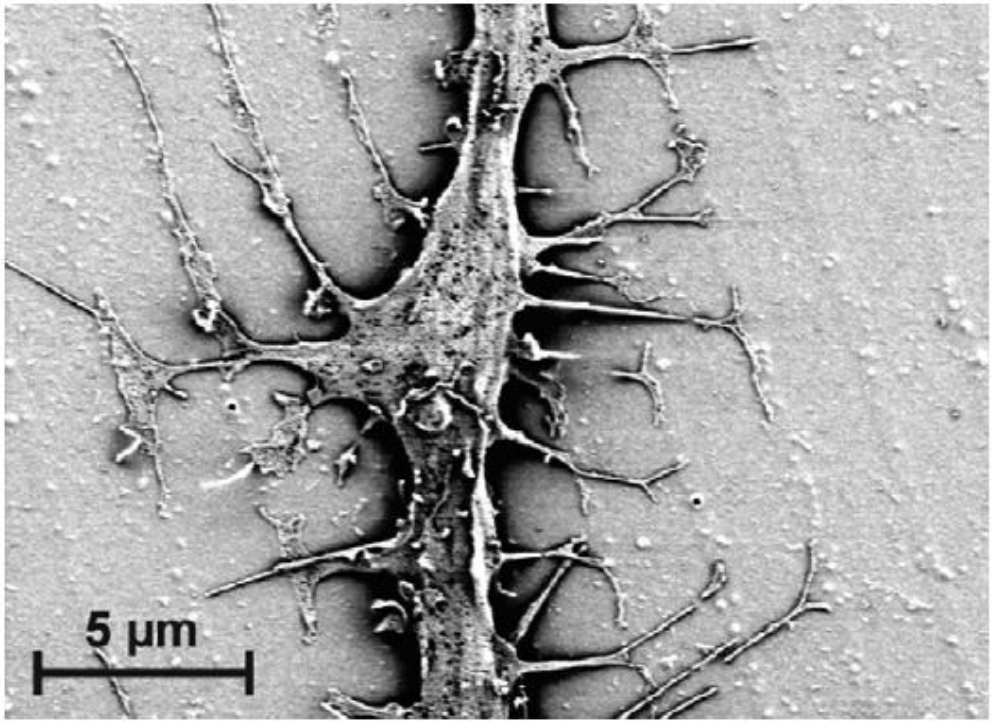

Fig. 4. Scanning electron micrograph of a cell process in a SAOS cell. Note the filopodia that try to come in contact with the oxide lines, 72 h after seeding on titanium/titanium oxide. Oxide lines 2 µm wide, 0.2 µm broad and 20 nm high.

We found that cells recognize electric charges on titanium/-oxide surfaces – especially the borders of the adjacent materials!

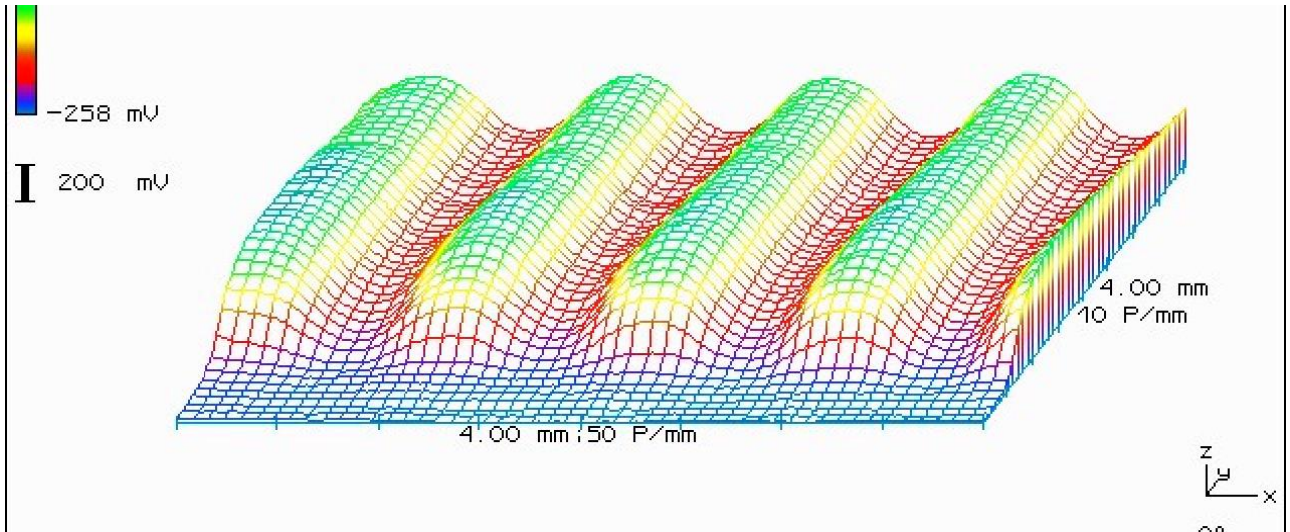

Electro-chemical fields arise not also during development but also during repair and regeneration processes…e.g. wound healing…

Levin et al. 2007

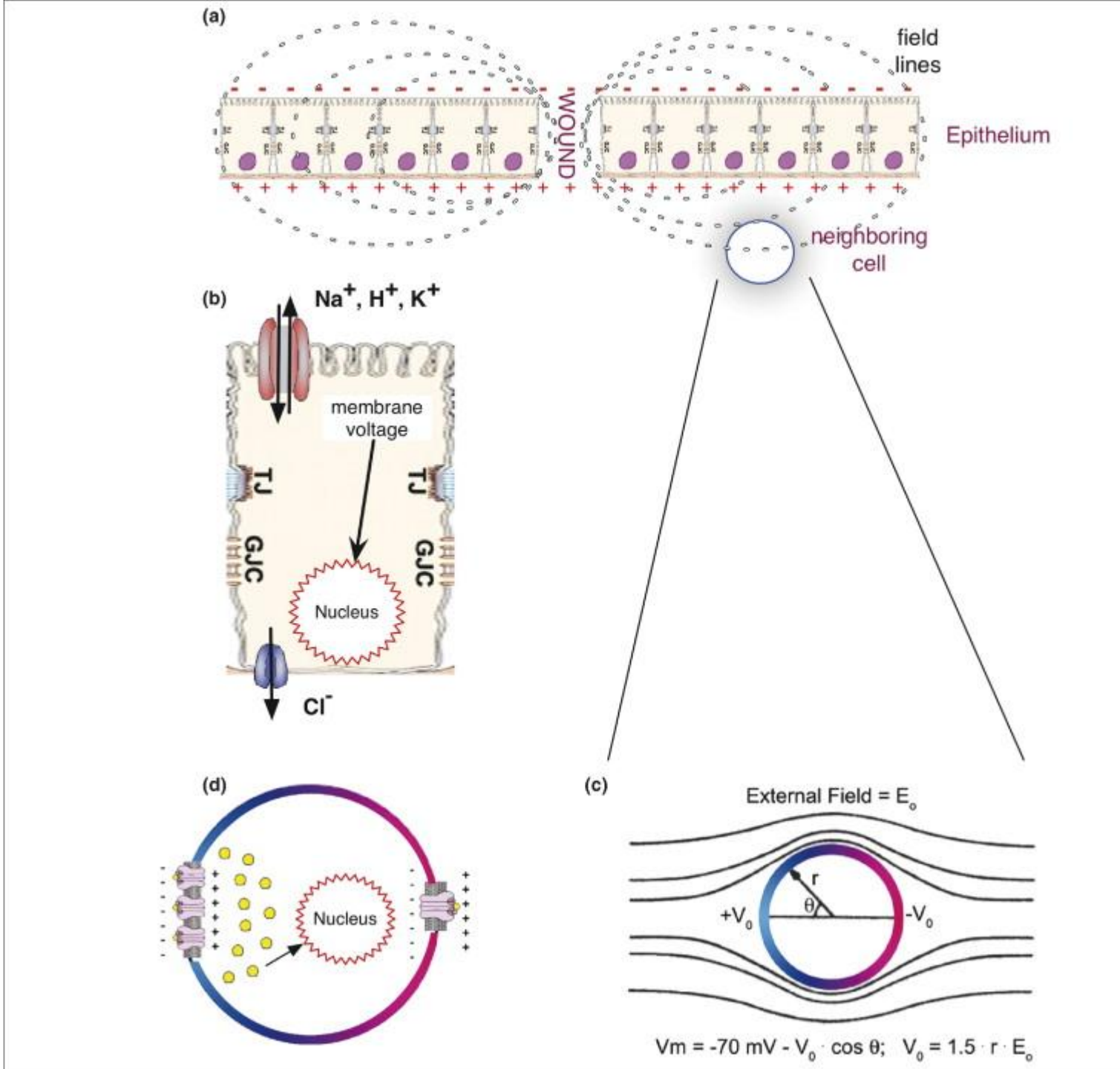

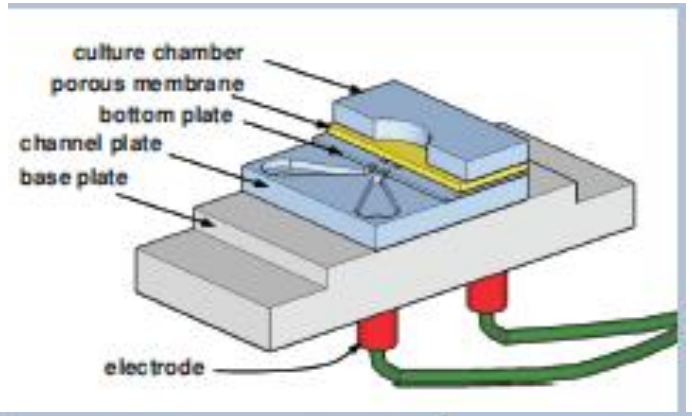

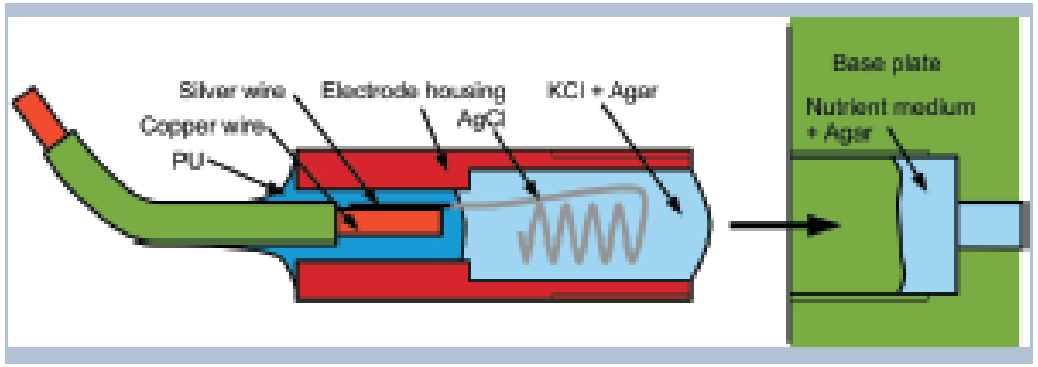

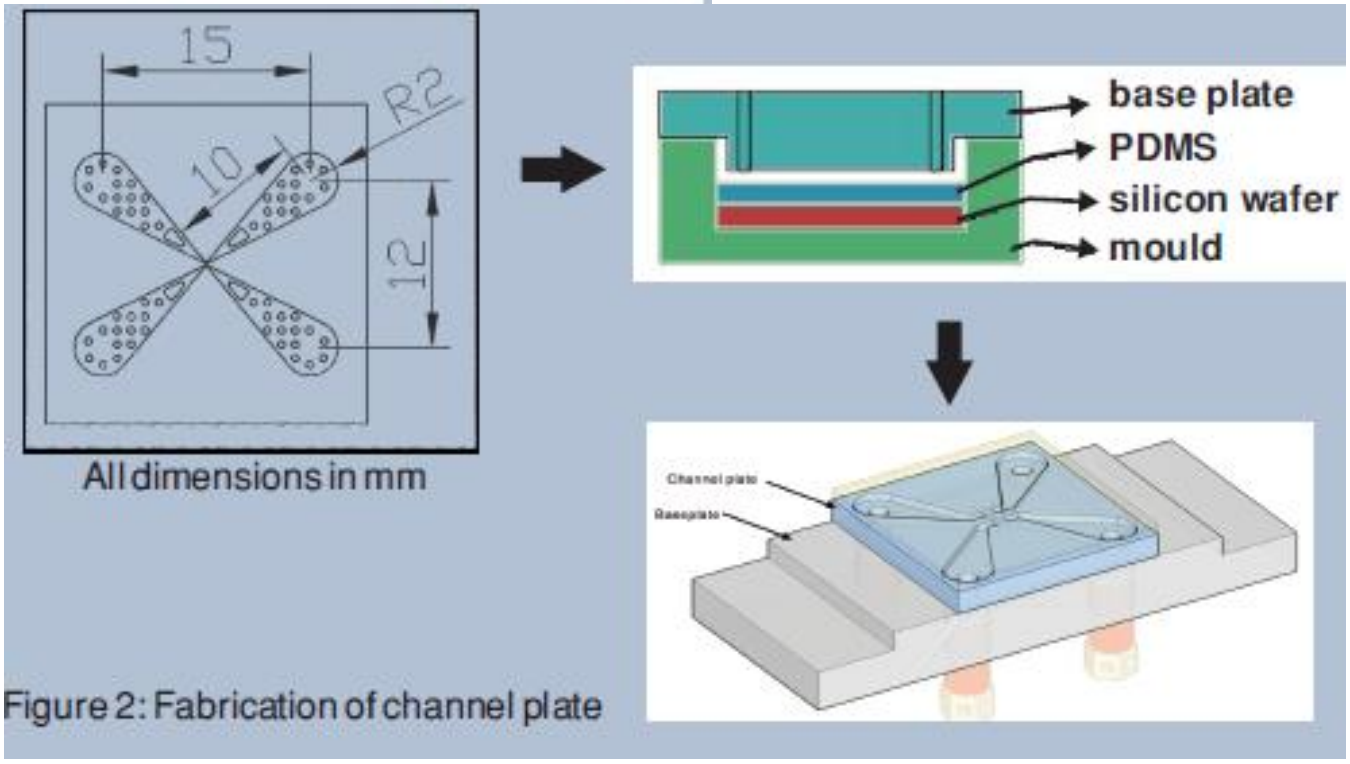

Figure 2: Fabrication of channel plate

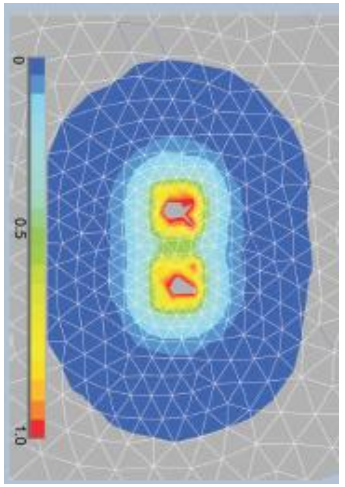

DC microelectrode array for investigating the intracellular ion changes.

Aryasomayajula A, Derix J, Perike S, Gerlach G, Funk RH.

Biosens Bioelectron. 2010 Jul 6.

Fig. 2. EDA sensor module. The device has a modular design and is shown with an optional radio transceiver mounted on top.

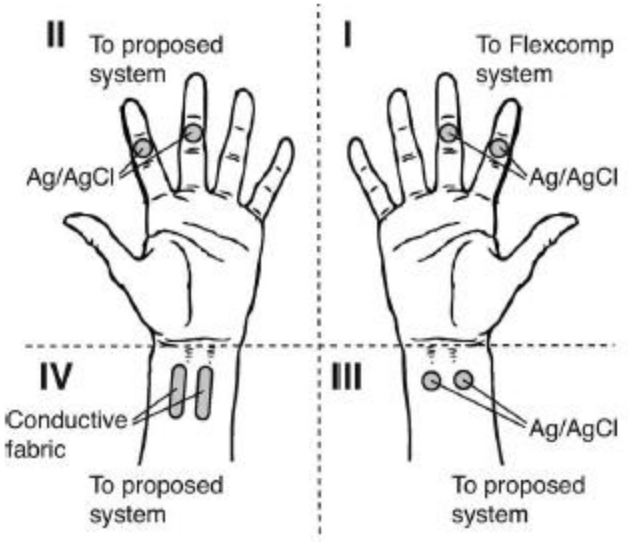

Fig. 4. Experimental setup. Measurements were recorded from (I) right fingers with the Flexcomp system, (II) left fingers with the proposed sensor module, (III) right distal forearm with the proposed sensor module using Ag/AgCl electrodes, and (IV) left distal forearm with the proposed sensor module using conductive fabric electrodes.

device is also inconspicuous, nonstigmatizing, and allows for discrete monitoring of EDA. Furthermore, the electronic module can be easily detached when the user desires to wash the wristband.

To date, there is no generally accepted standardization with respect to electrodermal recording sites [3]. The electrodes are commonly placed on the palmar surface of the hand, the most popular sites being the medial and distal phalanges of the fingers, and the thenar and hypothenar eminences (see Fig. 4). However, since both hands are often needed for manipulation, placement of electrodes on these sites is highly susceptible to motion artifacts and interferes with daily activities. Thus, we decided to use the ventral side of the distal forearms as our recording sites. We chose to use Ag/AgCl disc electrodes with contact areas of 1.0 cm^2 (Thought Technology, Ltd.) for our recordings, as recommended in the literature [33]. These elec-

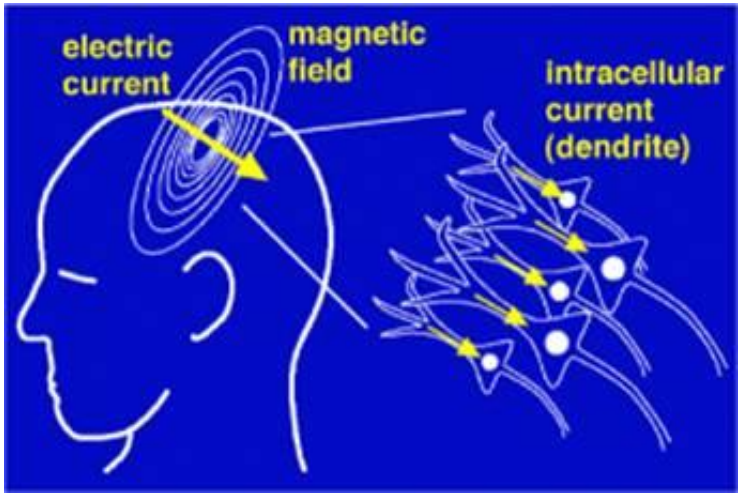
electric current
magnetic field
intracellular current (dendrite)

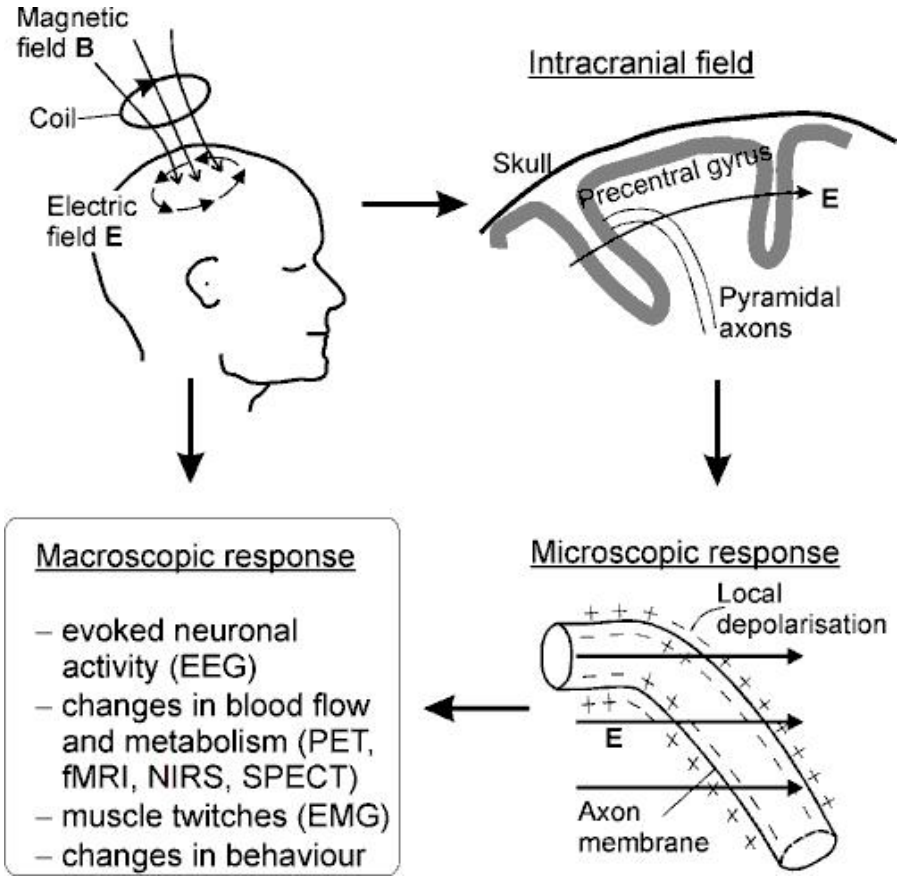
Magnetic field B
Coil
Electric field E
Intracranial field
Skull
Precentral gyrus
E
Pyramidal axons
Macroscopic response
– evoked neuronal activity (EEG)
– changes in blood flow and metabolism (PET, fMRI, NIRS, SPECT)
– muscle twitches (EMG)
– changes in behaviour
Microscopic response
Local depolarisation
E
Axon membrane

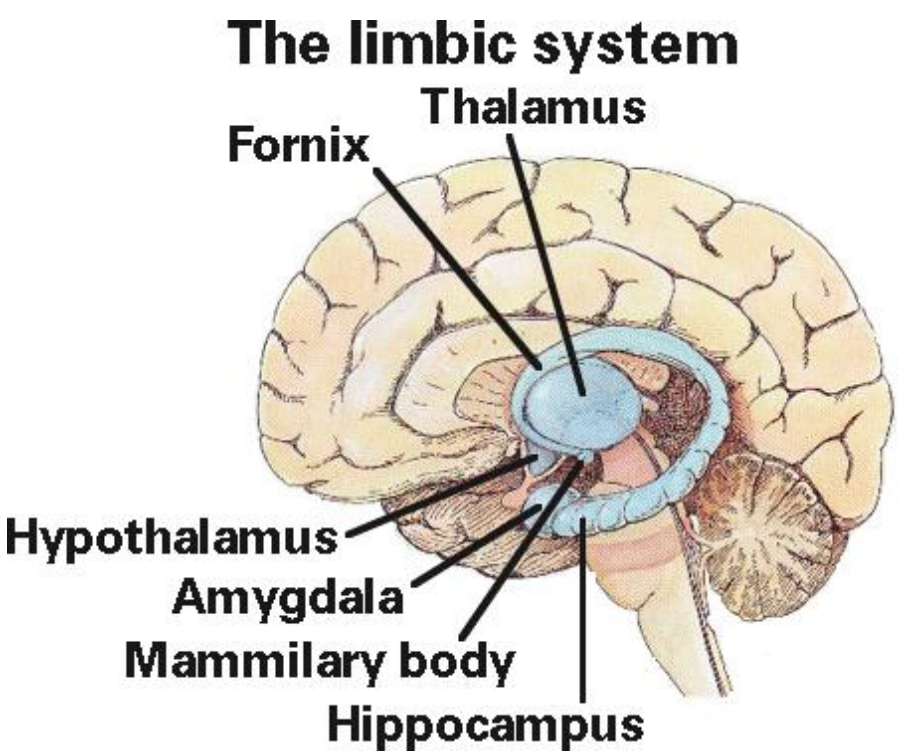
The limbic system
Thalamus
Fornix
Hypothalamus
Amygdala
Mammilary body
Hippocampus

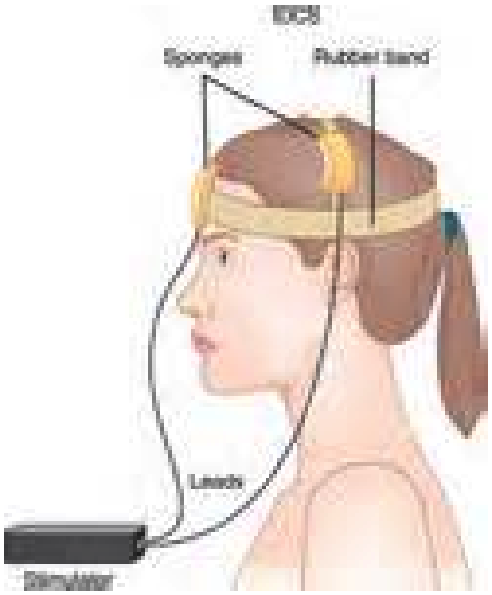
Sponges
Rubber band
Leads
Stimulator

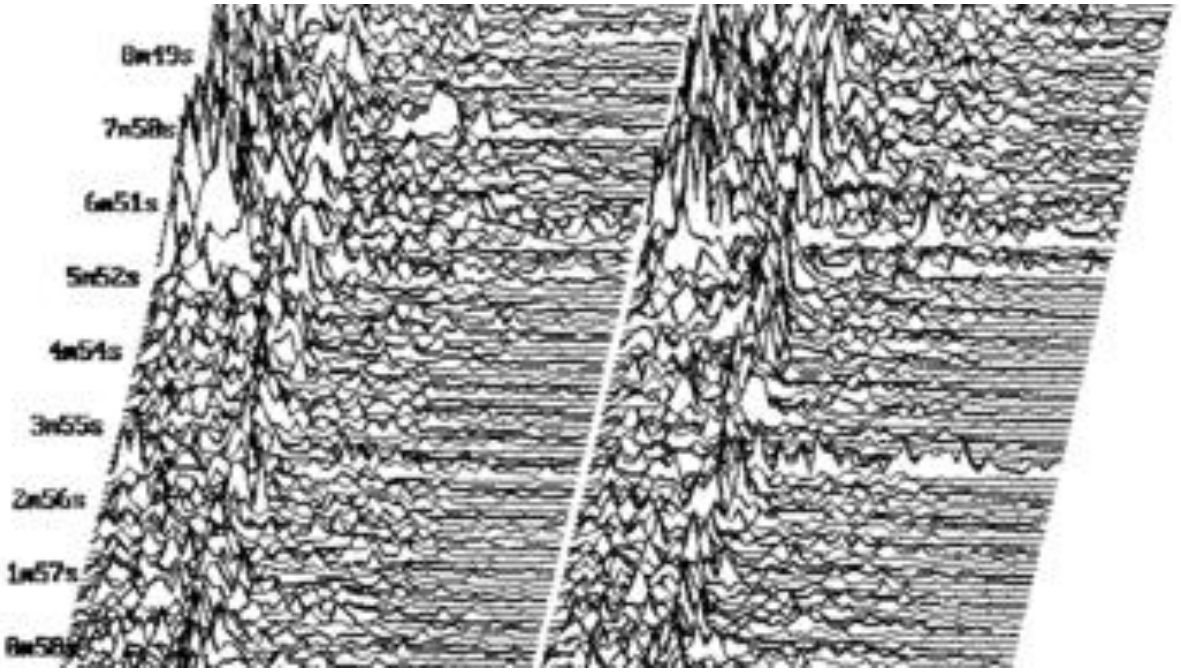

Das Cochlea Implantat (CI)

→ Hochgradige bis vollständige Schallempfindungsstörung
→ Ersetzt ausgefallene Innenohrfunktion
→ Hochgradige Schwerhörigkeit; Taubheit (kein Profit von Hörgeräten)
→ Elektrische Stimulation in der Cochlea

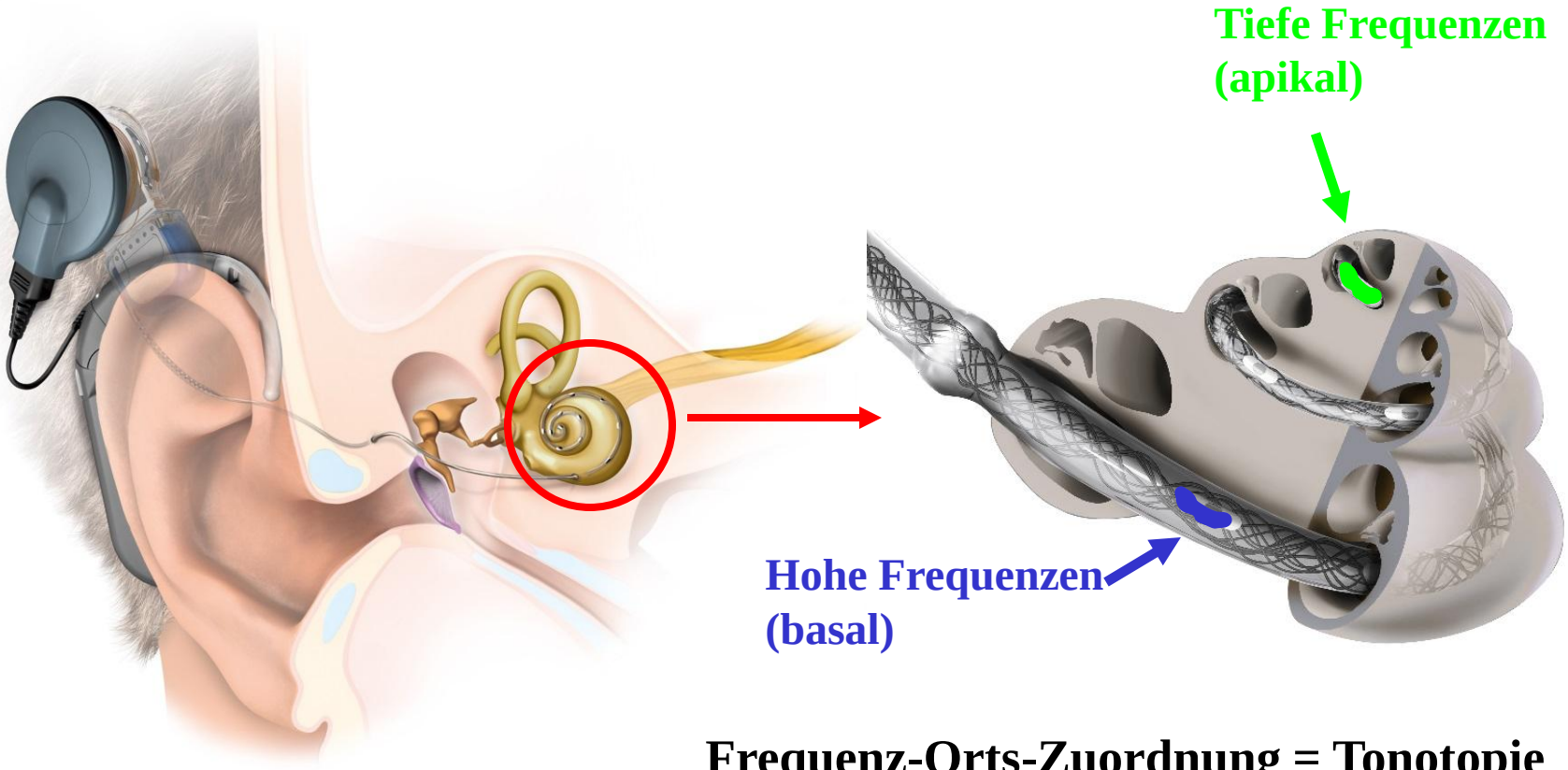

Frequenz-Orts-Zuordnung = Tonotopie

Zusammenfassung

- **Eignung der Digitalen Volumentomographie zur Insertionswinkelmessung**

MED-EL Flex20

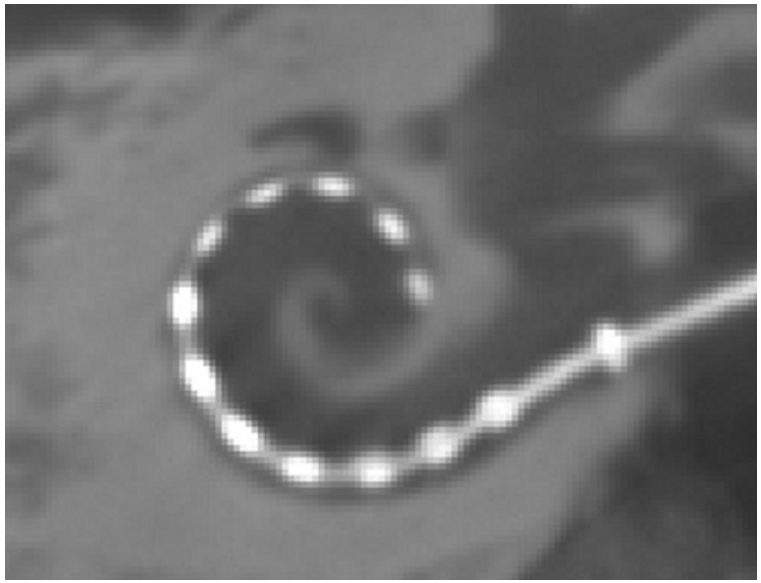

Cochlear Elektrode CI422

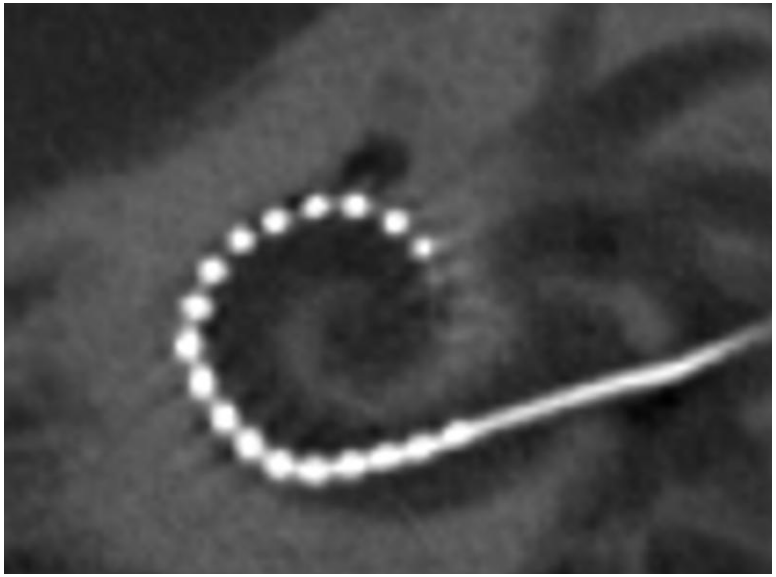

→angulare Position der einzelnen Elektroden

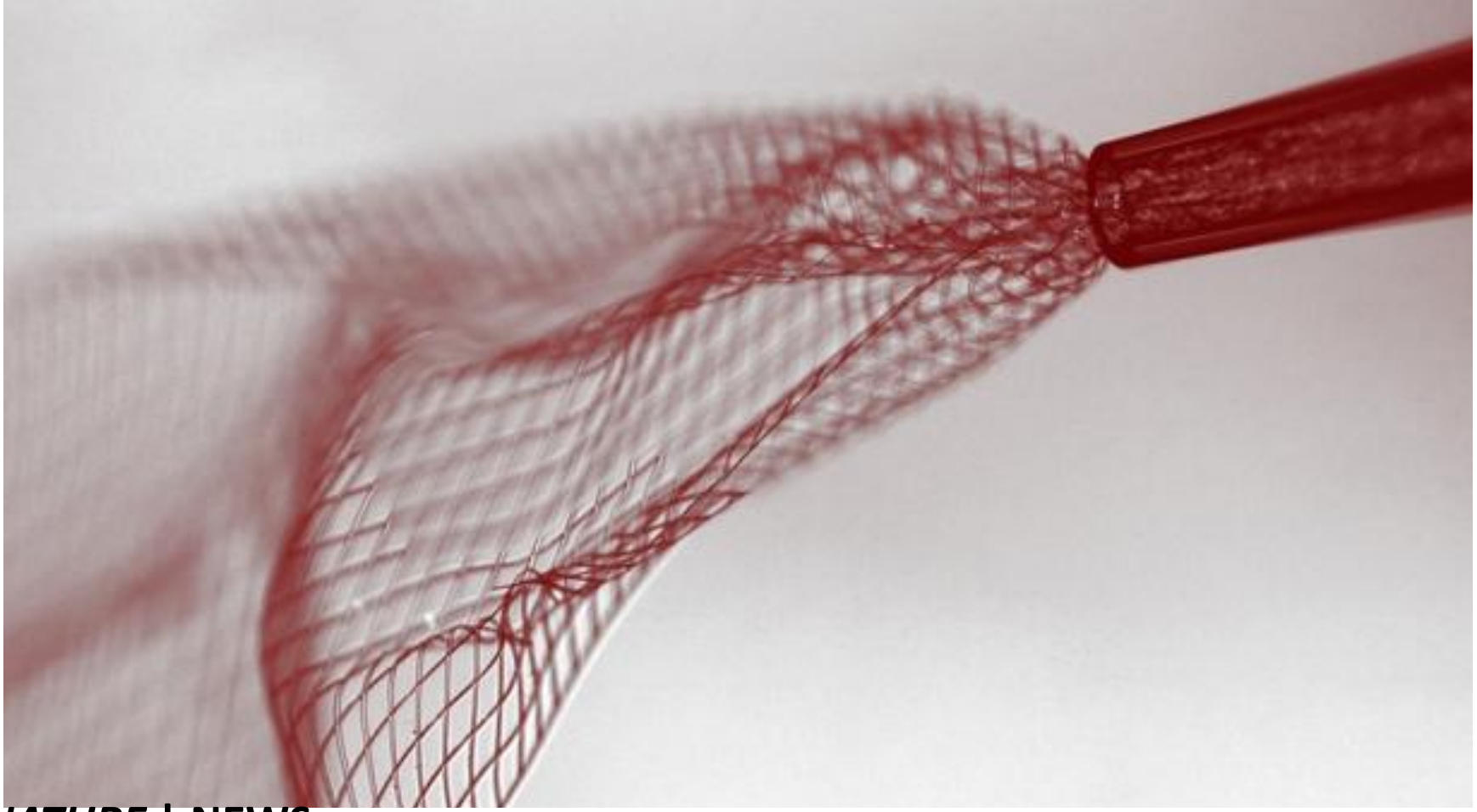

***NATURE* | NEWS**

Injectable brain implant spies on individual neurons

Electronic mesh has potential to unravel workings of mammalian brain.

Elizabeth Gibney

08 June 2015

This soft, conductive polymer mesh can be rolled up and injected into the brains of mice.

Development of Immunoassays Using Interferometric Real-Time Registration of Their Kinetics

A. V. Orlov, A. G. Burenin, V. O. Shipunova, A. A. Lizunova, B. G. Gorshkov, P. I. Nikitin, Moskov

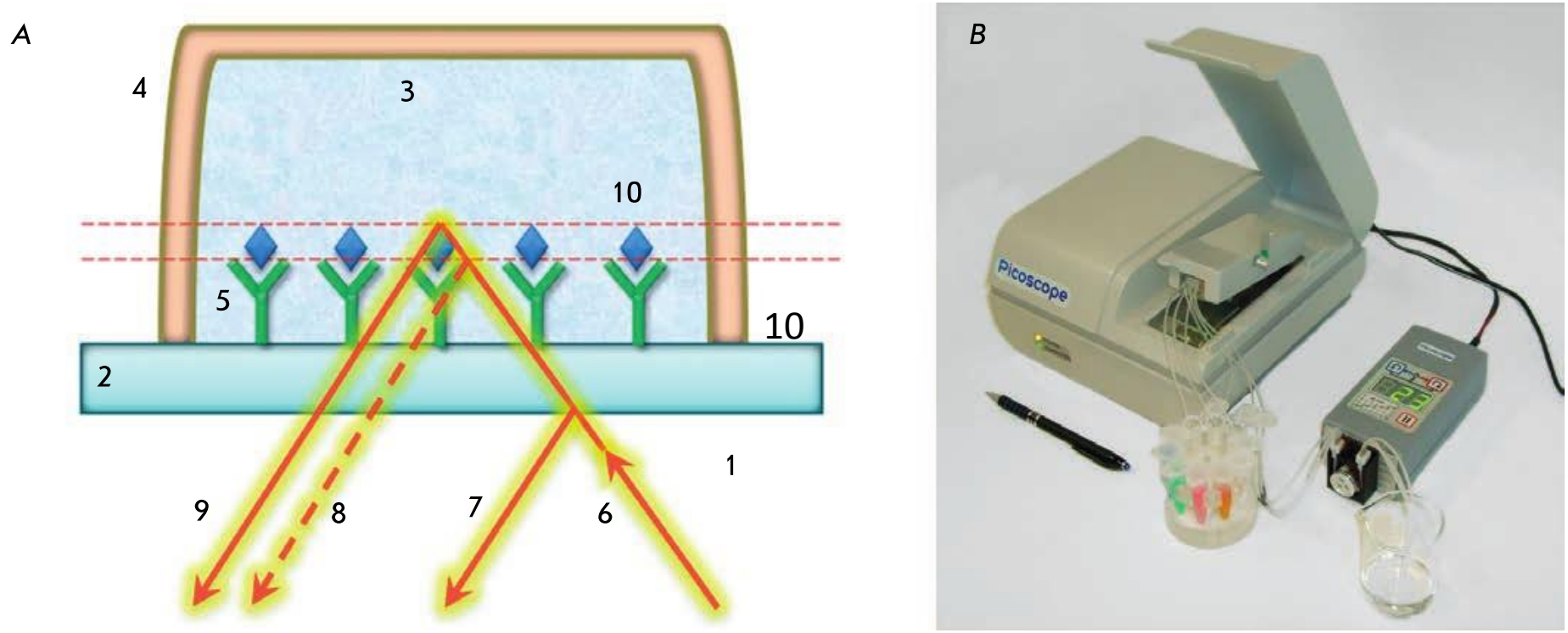

Fig. 1. The SCI principle. Changes in the optical thickness of a biolayer on a glass surface are recorded by a spectrum of interfering beams reflected from the sensor chip (A): 1 – air; 2 – microscopic glass cover slip; 3 – test solution; 4 – flow channel; 5 – receptor molecules; 6 – incident beam of superluminescent diode; 7,9 – reflected beams; 8 – position of the reflected beam before a biochemical reaction; 10 – detected biomolecules. (B): Photo of a three-channel Picoscope® biosensor

Johari S, Nock V, Alkaisi MM, Wang W. On-chip analysis of C. elegans muscular forces and locomotion patterns in microstructured environments. Lab Chip. 2013 May 7;13(9):1699-707.